

Spectral co-Clustering in Multi-layer Directed Networks

Wenqing Su¹, Xiao Guo^{*2}, Xiangyu Chang³, and Ying Yang^{*1}

¹Department of Mathematical Sciences, Tsinghua University

²School of Mathematics, Northwest University

³School of Management, Xi'an Jiaotong University

Abstract

Modern network analysis often involves multi-layer network data in which the nodes are aligned, and the edges on each layer represent one of the multiple relations among the nodes. Current literature on multi-layer network data is mostly limited to undirected relations. However, direct relations are more common and may introduce extra information. This study focuses on community detection (or clustering) in multi-layer directed networks. To take into account the asymmetry, a novel spectral-co-clustering-based algorithm is developed to detect *co-clusters*, which capture the sending patterns and receiving patterns of nodes, respectively. Specifically, the eigendecomposition of the *debiased* sum of Gram matrices over the layer-wise adjacency matrices is computed, followed by the *k*-means, where the sum of Gram matrices is used to avoid possible cancellation of clusters caused by direct summation. Theoretical analysis of the algorithm under the multi-layer stochastic co-block model is provided, where the common assumption that the cluster number is coupled with the rank of the model is relaxed. After a systematic analysis of the eigenvectors of the population version algorithm, the misclassification rates are derived, which show that multi-layers would bring benefits to the clustering performance. The experimental results of simulated data corroborate the theoretical predictions, and the analysis of a real-world trade network dataset provides interpretable results.

Keywords: Multi-layer directed networks, Co-clustering, Spectral methods, Bias-correction

**Corresponding authors.* Xiao Guo, xiaoguo@nwu.edu.cn. Ying Yang, yangying@tsinghua.edu.cn.

1 Introduction

Multi-layer network data arise naturally among various domains, where the nodes are the entities of interest and each network layer represents one of the multiple relations of the entities (Mucha et al., 2010; Holme and Saramäki, 2012; Kivelä et al., 2014; Boccaletti et al., 2014). A specific type of multi-layer network features identical sets of nodes across each layer, with no inter-layer connections. In this work, we refer to such networks as multi-layer networks, as in Paul and Chen (2020); Jing et al. (2021), though they are also called multiplex networks. For example, the gene co-expression multi-layer network consists of genes co-expressed at different developmental stages of the animal, and the gene expression patterns at different stages may differ yet remain highly correlated (Bakken et al., 2016; Zhang and Cao, 2017). The above example involves undirected relations. In real-world networks, more common relations are *directed*. For example, the Worldwide Food and Agricultural Trade (WFAT) multi-layer network consists of the direct trade relationships among the same set of countries across different commodities. Trade relationships concerning different commodities differ but are not entirely unrelated (De Domenico et al., 2015).

The multi-layer network has received considerable attention recently, see, e.g., Della Rossa et al. (2020); MacDonald et al. (2022); Huang et al. (2023) and references therein. Of particular interest is the community detection or clustering problem, where the goal is to partition the network nodes into disjoint *communities* or *clusters* with the help of multiple layers. We focus on the case where the underlying communities are consistent among all the layers. The community detection of multi-layer networks has been well-studied in the lens of multi-layer stochastic block models (multi-layer SBMs) (Han et al., 2015; Valles-Catala et al., 2016; Paul and Chen, 2016), namely, equipping each layer of the multi-layer network with a stochastic block model (SBM) (Holland et al., 1983). In an SBM, nodes are first partitioned into disjoint communities, and based on the community membership, the nodes are linked with probability specified by a *block probability matrix*. Specifically, Han et al. (2015) studied the asymptotic properties of spectral clustering and maximum likelihood estimation for multi-layer SBMs as the number of layers increases and the number of nodes remains fixed. Paul and Chen (2020) studied several spectral and matrix factorization-based

methods and provided theoretical guarantees under multi-layer SBMs. [Lei et al. \(2020\)](#) derived consistent results for a least squares estimation of community memberships and proved consistency of the global optima for general block structures without imposing the positive-semidefinite assumption for individual layers. [Lei and Lin \(2023\)](#) proposed a bias-adjusted spectral clustering for multi-layer SBMs and derived a novel aggregation strategy to avoid the community cancellation of different layers. Considering that different layers may have different community structures, [Jing et al. \(2021\)](#) introduced a mixture multi-layer SBM and proposed a tensor-based method to reveal both memberships of layers and memberships of nodes. [Wang et al. \(2021\)](#) and [Fu and Hu \(2023\)](#) studied the recovery of community structures in multi-layer SBMs using the pseudo-likelihood method. Also see [Bhattacharyya and Chatterjee \(2018\)](#); [Pensky and Zhang \(2019\)](#); [Arroyo et al. \(2021\)](#); [Noroozi and Pensky \(2022\)](#); among others.

Despite the great efforts on the community detection of multi-layer networks, the following two issues remain to be tackled. First, existing literature is mostly limited to undirected networks. For directed networks, the most common approach is to simply ignore edge directions and use the methods developed for multi-layer undirected networks. However, this simplistic technique is unsatisfactory since the potentially useful information contained in edge directions is not retained. For example, in the WFAT multi-layer network, the trade transactions among countries include both import and export, which is quite different for even a single country. Therefore, clustering nodes regardless of their edge directions would be coarse. To incorporate the asymmetry of directed networks, instead of partitioning the nodes into one set of clusters, it is more reasonable to *co-cluster* the network nodes ([Malliaros and Vazirgiannis, 2013](#); [Rohe et al., 2016](#); [Zhang et al., 2022](#)). That is, clustering the nodes in two ways to obtain *co-clusters*, namely, the row clusters (or the sending clusters) and the column clusters (or the receiving clusters). The nodes in the same row (column) cluster have similar sending (receiving) patterns. Hence, the community detection of multi-layer directed networks should be in the context of co-clustering.

Second, most existing literature on SBMs assumes that the population matrix has rank coupled with the number of underlying communities. That is, the block probability matrix is assumed to be of *full* rank. Such assumption brings benefits to the algebraic properties

of the matrices arising from SBMs. However, this assumption is not necessarily met by practical tasks. In the context of multi-layer SBMs, this assumption is inherited in that the population matrix, for example, the *sum* of each layer-wise SBM, is commonly assumed to be of rank equaling the number of communities, although each *layer-wise* SBM does not necessarily satisfy the assumption (Paul and Chen, 2020). In the context of single-layer SBMs, Tang et al. (2022) studied the asymptotic normality of the estimated block probability matrix without the full rank assumption, while their asymptotic theoretical machinery is not directly applicable to our non-asymptotic justification of the clustering performance. Thus, to meet practical needs, it is desirable to study the theoretical properties of the population model of multi-layer directed networks in the rank-deficient regime.

Motivated by the above problems, we study the problem of co-clustering the multi-layer directed network. We typically assume that each layer of the network is generated from a stochastic co-block model (ScBM) (Rohe et al., 2016), where the underlying row clusters and column clusters are not necessarily the same. Following convention, we call the model over all layers the *multi-layer* ScBM. The first contribution of this paper is a neat, flexible, and computationally efficient spectral-clustering-based algorithm for co-clustering the multi-layer directed network. To avoid possible cancellation of clusters among layers, we use the *sum of Gram* (SoG) matrices of the row (column) spaces of the layer-wise adjacency matrices as the algorithm’s target matrix in order to detect row (column) clusters. Then, we perform a bias-correction on the two-way SoG matrices to remove the bias that comes from their diagonal entries. After that, we apply the spectral clustering to the two debiased SoG matrices with possibly different cluster numbers. As the leading eigenvectors approximate the row and column spaces of the two debiased SoG matrices, respectively, it is expected that the resulting two sets of clusters contain nodes with similar sending and receiving patterns, respectively. To the best of our knowledge, this is the first work to study the community detection problem for multi-layer directed networks.

The second contribution of this work is that we systematically study the algebraic properties of the population version of SoG matrices whose block probability matrix is *not* necessarily of full rank. In particular, we provide interpretable conditions under which the eigendecomposition (i.e., the first step of the spectral clustering) of the population version

of SoG matrices would reveal the underlying communities in multi-layer ScBMs. Based on these findings, we provide rigorous analysis of the consistency of the community estimates. Specifically, we use the decoupling techniques (de la Peña and Montgomery-Smith, 1995; Lei and Lin, 2023) to derive the concentration inequalities of the sum of quadratic asymmetric matrices. We use the derived inequalities to bound the misclassification rate of the row and column clusters, respectively.

The remainder of the paper is organized as follows. Section 2 presents the model for multi-layer directed networks and investigates its algebraic properties. Section 3 develops the debiased spectral co-clustering algorithm and proves its consistency. Section 4 illustrates the finite sample performance of the proposed method via simulations. Section 5 includes a real-world application of the proposed method to the WFAT dataset. Section 6 concludes the paper and provides possible extensions. Technical proofs are included in the Appendix.

2 The multi-layer ScBM and its algebraic properties

In this section, we first present the multi-layer ScBM for modeling the multi-layer directed network. Next, we study its algebraic properties for understanding the population-wise clustering behavior of spectral co-clustering based on the SoG matrices.

Notes and notation: We use $[n]$ to denote the set $\{1, \dots, n\}$. For a matrix $M \in \mathbb{R}^{m \times n}$ and index $i \in [m]$ and $j \in [n]$, M_{i*} and M_{*j} denote the i th row and j th column of M , respectively. $\|M\|_F$, $\|M\|_{\max}$, $\|M\|_{1,\infty}$, and $\|M\|_{2,\infty}$ denote the Frobenius norm, the element-wise maximum absolute value, the maximum row-wise l_1 norm and the maximum row-wise l_2 norm of a given matrix M , respectively. In addition, $\|\cdot\|_2$ denotes the Euclidean norm of a vector or the spectral norm of a matrix. We will use c, c_0, c_1 , and more generally c_i , to denote constants that vary across different contexts. Following convention, we will use clusters and communities interchangeably.

2.1 Multi-layer ScBMs

Consider the multi-layer directed network with L -layers and n common nodes, whose adjacency matrices are denoted by A_l , where $A_l \in \{0, 1\}^{n \times n}$ for all $1 \leq l \leq L$. We assume that all

the layers share common row and column clusters but with possibly different edge densities. In particular, suppose that n nodes are assigned to K_y non-overlapping row clusters and K_z non-overlapping column clusters, respectively. The number of nodes in the row (column) cluster $k \in [K_y]$ ($k \in [K_z]$) is denoted by n_k^y (n_k^z). For $i \in [n]$, the row (column) cluster assignment of node i is given by $g_i^y \in [K_y]$ ($g_i^z \in [K_z]$). Given the cluster assignment, we assume the layer-wise networks are generated independently from the following ScBM (Rohe et al., 2016). That is, for any pair of nodes $i \neq j$ (with $j \in [n]$) and any layer $l \in [L]$, each $A_{l,ij}$ is generated independently according to

$$A_{l,ij} \sim \text{Bernoulli}(\rho B_{l,g_i^y g_j^z}), \quad (1)$$

where $\rho \in (0, 1]$ is an overall edge density parameter, $B_l \in [0, 1]^{K_y \times K_z}$ denotes the *heterogeneous* block probability matrix indicating the community-wise edge probabilities in each l . While for any $l \in [L]$ and $i = j$, $A_{l,ii} = 0$. It can be seen from (1) that nodes in a common row (column) cluster are stochastically equivalent senders (receivers) in the sense that they send out (receive) an edge to a third node with equal probabilities. Putting together the L layer-wise networks $\{A_l\}_{l=1}^L$, we say that the multi-layer network is generated from the multi-layer ScBM.

Throughout this paper, we assume that the number of communities is fixed and the community sizes are balanced. Specifically, we make the following Assumption 1.

Assumption 1. *Both the number of row clusters K_y and the number of column clusters K_z are fixed. The community sizes are balanced, that is, there exists a constant $c_0 \geq 1$ such that each row cluster size is in $[c_0^{-1}n/K_y, c_0n/K_y]$ and each column cluster size is in $[c_0^{-1}n/K_z, c_0n/K_z]$.*

2.2 Algebraic properties of multi-layer ScBMs

It is essential to investigate the algebraic properties of multi-layer ScBMs in order to understand the rationality of a clustering algorithm from the angle of population. Before that, we must specify the clustering algorithm.

For the single-layer ScBM, *spectral co-clustering* (Rohe et al., 2016; Guo et al., 2023) is a popular and effective algorithm, which first computes the singular value decomposition

(SVD) of a matrix, say the adjacency matrix A , and then implements k -means on the left and right singular vectors to obtain the row and column clusters, respectively. For the multi-layer ScBM, we also proceed to develop the spectral co-clustering-based method to detect the co-clusters. It is natural to use the summation matrix $\sum_{l=1}^L A_l$ as the input of spectral co-clustering. However, such direct summation may lead to cancellation of clusters. For example, suppose $B_1 := \begin{bmatrix} a & b \\ c & d \end{bmatrix}$ and $B_2 := \begin{bmatrix} b & a \\ d & c \end{bmatrix}$, the sum $B_1 + B_2 = \begin{bmatrix} a+b & a+b \\ c+d & c+d \end{bmatrix}$ results in identical columns and thus provides no signal for the column clusters. Considering that the ij th entry of $A_l A_l^T$ (resp. $A_l^T A_l$) counts the number of common children (resp. parents) nodes of nodes i and j , we proceed to use the leading eigenvectors of SoG matrices $\sum_{l=1}^L A_l A_l^T$ (resp. $\sum_{l=1}^L A_l^T A_l$) as the input of subsequent k -means clustering, in order to obtain the row (resp. column) clusters of nodes with similar sending (resp. receiving) patterns. We will modify the algorithm in the next section.

In the sequel, we investigate the theoretical properties of the eigenvectors of the population version of $\sum_{l=1}^L A_l A_l^T$ and $\sum_{l=1}^L A_l^T A_l$. Before that, we give some notations. Let $Y \in \{0, 1\}^{n \times K_y}$ and $Z \in \{0, 1\}^{n \times K_z}$ be the row and column membership matrices, respectively, where each row consists of all 0's except one 1. In particular, $Y_{ig_i^y} = 1$ and $Z_{ig_i^z} = 1$ for each i . For $l \in [L]$, denote $\mathcal{P}_l = \rho Y B_l Z^T \in [0, 1]^{n \times n}$, it is easy to see that \mathcal{P}_l serve as the population matrices for A_l , in the sense that $\mathcal{P}_l - \text{diag}(\mathcal{P}_l) = \mathbb{E}(A_l)$. The subsequent lemmas indicate that the rows of the eigenvectors of $\sum_{l=1}^L \mathcal{P}_l \mathcal{P}_l^T$ and $\sum_{l=1}^L \mathcal{P}_l^T \mathcal{P}_l$ could reveal the true row and column clusters, respectively. The proofs of the lemmas are provided in Appendix B. We begin by considering the row clusters.

Lemma 1. *Consider the multi-layer ScBM parameterized by $(Y_{n \times K_y}, Z_{n \times K_z}, \rho \{B_l\}_{l=1}^L)$. Suppose $\text{rank}(\sum_{l=1}^L B_l B_l^T) = K (K \leq K_y)$. Denote the eigendecomposition of $\sum_{l=1}^L \mathcal{P}_l \mathcal{P}_l^T$ by $U \Lambda^R U^T$, where U is an $n \times K$ matrix with orthonormal columns and Λ^R is a $K \times K$ diagonal matrix. Denote the eigendecomposition of $\Delta_y \sum_{l=1}^L B_l \Delta_z^2 B_l^T \Delta_y$ by $Q^R D^R Q^{RT}$, where $\Delta_y := \text{diag}(\sqrt{n_1^y}, \dots, \sqrt{n_{K_y}^y})$ and $\Delta_z := \text{diag}(\sqrt{n_1^z}, \dots, \sqrt{n_{K_z}^z})$. Then we have*

- (a) *If $\sum_{l=1}^L B_l B_l^T$ is of full rank, i.e., $K = K_y$, then $Y_{i*} = Y_{j*}$ if and only if $U_{i*} = U_{j*}$. Otherwise, for any $Y_{i*} \neq Y_{j*}$, we have $\|U_{i*} - U_{j*}\|_2 = \sqrt{n_{g_i^y}^{-1} + n_{g_j^y}^{-1}}$.*
- (b) *If $\sum_{l=1}^L B_l B_l^T$ is rank-deficient, i.e., $K < K_y$, then for $Y_{i*} = Y_{j*}$, we have $U_{i*} = U_{j*}$.*

Otherwise, if $\Delta_y^{-1}Q^R$ has mutually distinct rows and there exists a deterministic positive sequence $\{\zeta_n\}_{n \geq 1}$ such that

$$\min_{1 \leq k \neq k' \leq K_y} \left\| \frac{Q_{k*}^R}{\sqrt{n_k}} - \frac{Q_{k'*}^R}{\sqrt{n_{k'}}} \right\|_2 \geq \zeta_n, \quad (2)$$

then for any $Y_{i*} \neq Y_{j*}$, we have $\|U_{i*} - U_{j*}\|_2 \geq \zeta_n$.

Remark 1. Note that in the literature on ScBM, the row cluster number K_y , the column cluster number K_z and the rank K of population matrix are commonly coupled, say, it is often assumed that $K = K_y \leq K_z$ or $K = K_z \leq K_y$ (Rohe et al., 2016). We here relax this assumption and make the model more practical.

Lemma 1 shows that when two nodes are in the same row cluster, the corresponding rows of U coincide. Conversely, if the nodes do not belong to the same row cluster, a gap is present between their corresponding rows in U . As we will see, this brings confidence to the success of the spectral co-clustering using the sample version of $\sum_{l=1}^L \mathcal{P}_l \mathcal{P}_l^T$. Note that in the rank-deficient case, we additionally require (2) holds to ensure that two rows of U are separable for nodes with different row clusters.

It is desirable to study the sufficient and interpretable condition to satisfy (2). Define a flattened block probability matrix $B^R := [B_1, \dots, B_L] \in [0, 1]^{K_y \times LK_z}$, where the k th row contains the overall sending pattern of the k th row cluster to each of the column clusters across all layers. The following lemma provides an explicit condition on B^R such that (2) holds.

Lemma 2. Under the same multi-layer ScBM as in Lemma 1 and Assumption 1, if B^R satisfies

$$\min_{1 \leq k \neq k' \leq K_y} c_0^{-1} L^{-1} \langle B_{k*}^R, B_{k*}^R \rangle + c_0^{-1} L^{-1} \langle B_{k'*}^R, B_{k'*}^R \rangle - 2c_0 L^{-1} \langle B_{k*}^R, B_{k'*}^R \rangle \geq c_0^2 n \zeta_n^2, \quad (3)$$

then condition (2) is met. Here ζ_n is the RHS of (2) and $c_0 \geq 1$ is the constant specified in Assumption 1.

Lemma 2 is interpretable in that it requires certain difference between any two row pairs in B^R . To see this more clearly, if the column clusters are absolutely balanced, then it turns out that $c_0 = 1$ and the LHS of (3) is equivalent to the Euclidean distance (divided by L) of two different rows of B^R .

Remark 2. It is worth mentioning that we only require the overall difference of each row cluster pair. Hence, some layers with weak cluster signal can borrow the strength from other layers with strong cluster signal, which shows the benefit of combining the layer-wise networks.

The aforementioned results focus on the row clusters. For the column clusters, we can derive similar results if we study instead $\sum_{l=1}^L \mathcal{P}_l^T \mathcal{P}_l$.

Lemma 3. Under the same multi-layer ScBM as in Lemma 1 and suppose $\text{rank}(\sum_{l=1}^L B_l^T B_l) = K' (K' \leq K_z)$. Denote the eigendecomposition of $\sum_{l=1}^L \mathcal{P}_l^T \mathcal{P}_l$ by $V \Lambda^C V^T$, where V is an $n \times K'$ matrix with orthonormal columns and Λ^C is a $K' \times K'$ diagonal matrix. Denote the eigendecomposition of $\Delta_z \sum_{l=1}^L B_l^T \Delta_y^2 B_l \Delta_z$ by $Q^C D^C Q^{C^T}$. Then we have

(a) If $\sum_{l=1}^L B_l^T B_l$ is of full rank, i.e., $K' = K_z$, then $Z_{i^*} = Z_{j^*}$ if and only if $V_{i^*} = V_{j^*}$. Otherwise, for any $Z_{i^*} \neq Z_{j^*}$, we have $\|V_{i^*} - V_{j^*}\|_2 = \sqrt{n_{g_i^z}^{-1} + n_{g_j^z}^{-1}}$.

(b) If $\sum_{l=1}^L B_l^T B_l$ is rank-deficient, i.e., $K' < K_z$, then for $Z_{i^*} = Z_{j^*}$, we have $V_{i^*} = V_{j^*}$. Otherwise, if $\Delta_z^{-1} Q^C$ has mutually distinct rows and there exists a deterministic positive sequence $\{\xi_n\}_{n \geq 1}$ such that

$$\min_{1 \leq k \neq k' \leq K_z} \left\| \frac{Q_{k^*}^C}{\sqrt{n_k}} - \frac{Q_{k'^*}^C}{\sqrt{n_{k'}}} \right\|_2 \geq \xi_n, \quad (4)$$

then for any $Z_{i^*} \neq Z_{j^*}$, we have $\|V_{i^*} - V_{j^*}\|_2 \geq \xi_n$.

Lemma 3 shows that the leading eigenvectors of $\sum_{l=1}^L \mathcal{P}_l^T \mathcal{P}_l$ can expose the true underlying column clusters, where when $\sum_{l=1}^L B_l^T B_l$ is rank-deficient, we need extra condition (4). In the following Lemma 4, we provide a sufficient condition under which (4) holds. In particular, when $\sum_{l=1}^L B_l^T B_l$ is rank-deficient, we provide an interpretable condition on the flattened matrix $B^C := [B_1^T, \dots, B_L^T] \in [0, 1]^{K_z \times LK_y}$ which is sufficient for (4).

Lemma 4. Under the same multi-layer ScBM as in Lemma 3 and Assumption 1, if B^C satisfies

$$\min_{1 \leq k \neq k' \leq K_z} c_0^{-1} L^{-1} \langle B_{k^*}^C, B_{k^*}^C \rangle + c_0^{-1} L^{-1} \langle B_{k'^*}^C, B_{k'^*}^C \rangle - 2c_0 L^{-1} \langle B_{k^*}^C, B_{k'^*}^C \rangle \geq c_0^2 n \xi_n^2,$$

then (4) holds. Here ξ_n is the RHS of (4) and $c_0 \geq 1$ is the constant specified in Assumption 1.

3 Debiased spectral co-clustering and its consistency

In this section, we formally present the spectral-co-clustering algorithm based on the SoG matrices, where we provide a bias-adjustment strategy to remove the bias of the SoG matrix. Then we study its theoretical properties in terms of misclassification rate.

3.1 Debiased spectral co-clustering

We begin by considering the row clusters. As illustrated in Section 2, we have shown that $\sum_{l=1}^L A_l A_l^T$ is a good surrogate of $\sum_{l=1}^L A_l$ for avoiding possible row clustering cancellation, and we provide theoretical support that the population-wise matrix $\sum_{l=1}^L \mathcal{P}_l \mathcal{P}_l^T$ has eigenvectors that can reveal the true underlying row clusters, recalling that $\mathcal{P}_l - \text{diag}(\mathcal{P}_l) = \mathbb{E}(A_l)$. However, similar to the undirected case studied in [Lei and Lin \(2023\)](#), we will see that $\sum_{l=1}^L A_l A_l^T$ turns out to be a biased estimate of $\sum_{l=1}^L \mathcal{P}_l \mathcal{P}_l^T$.

For notational simplicity, denote $\bar{P}_l := \mathcal{P}_l - \text{diag}(\mathcal{P}_l)$ and denote $X_l := A_l - \bar{P}_l$. Then we can decompose the deviation of $\sum_{l=1}^L A_l A_l^T$ from $\sum_{l=1}^L \mathcal{P}_l \mathcal{P}_l^T$ as

$$\sum_{l=1}^L A_l A_l^T - \sum_{l=1}^L \mathcal{P}_l \mathcal{P}_l^T := N_1 + N_2 + N_3 + \text{diag}\left(\sum_{l=1}^L X_l X_l^T\right), \quad (5)$$

where

$$\begin{aligned} N_1 &= \sum_{l=1}^L (\text{diag}^2(\mathcal{P}_l) - \mathcal{P}_l \text{diag}(\mathcal{P}_l) - \text{diag}(\mathcal{P}_l) \mathcal{P}_l^T), \\ N_2 &= \sum_{l=1}^L (\bar{P}_l X_l^T + X_l \bar{P}_l^T), \\ N_3 &= \sum_{l=1}^L X_l X_l^T - \text{diag}\left(\sum_{l=1}^L X_l X_l^T\right). \end{aligned} \quad (6)$$

The terms N_1 , N_2 and N_3 are all relatively small. While for $\text{diag}(\sum_{l=1}^L X_l X_l^T)$, we have the following argument for its i th diagonal element,

$$\begin{aligned} (\text{diag}\left(\sum_{l=1}^L X_l X_l^T\right))_{ii} &= \sum_{l=1}^L \sum_{j=1}^n \bar{P}_{l,ij}^2 \mathbb{I}(A_{l,ij} = 0) + \sum_{l=1}^L \sum_{j=1}^n (1 - \bar{P}_{l,ij})^2 \mathbb{I}(A_{l,ij} = 1) \\ &\leq Ln \max_{l,ij} \bar{P}_{l,ij}^2 + \sum_{l=1}^L d_{l,i}^{\text{out}}, \end{aligned} \quad (7)$$

where $d_{l,i}^{out} := \sum_{j=1}^n A_{l,ij}$ is the out-degree of node i in layer l . Note that the expectation of $\sum_{l=1}^L d_{l,i}^{out}$ is of the same order as $Ln \max_{l,ij} \bar{P}_{l,ij}$, which dominates the first term $Ln \max_{l,ij} \bar{P}_{l,ij}^2$ under the sparse regime where $\bar{P}_{l,ij} = o(1)$. As a result, to reduce the upper bound, we can directly minus $\sum_{l=1}^L d_{l,i}^{out}$ from both sides of (7). Specifically, define the row-wise bias-adjusted SoG matrix by

$$S^R = \sum_{l=1}^L (A_l A_l^T - D_l^{out}), \quad (8)$$

where $D_l^{out} = \text{diag}(d_{l,1}^{out}, \dots, d_{l,n}^{out})$. Then, the row clusters partition can be obtained by performing k -means on the row of the K leading eigenvectors of S^R .

Similarly, for the column clusters, we can define the column-wise bias-adjusted SoG matrix by

$$S^C = \sum_{l=1}^L (A_l^T A_l - D_l^{in}), \quad (9)$$

where $D_l^{in} = \text{diag}(d_{l,1}^{in}, \dots, d_{l,n}^{in})$ with $d_{l,j}^{in} := \sum_{i=1}^n A_{l,ij}$. The column clusters partition can then be obtained by applying k -means on the row of the K' leading eigenvectors of S^C .

We summarize the spectral co-clustering based on the debiased SoG matrices in Algorithm 1, and in what follows, we will refer to the algorithm by DSoG.

Algorithm 1 Spectral co-clustering based on the debiased sum of Gram matrices (DSoG)

Input: Adjacency matrices A_1, \dots, A_L , row cluster number K_y , column cluster number K_z , target ranks $K (K \leq K_y)$ and $K' (K' \leq K_z)$;

Output: Estimated row membership matrix \hat{Y} , and column membership matrix \hat{Z} ;

- 1: Find the K leading eigenvectors \hat{U} of S^R in (8), and the K' leading eigenvectors \hat{V} of S^C in (9).
 - 2: Treat each row of \hat{U} as a point in $\mathbb{R}^{n \times K}$ and run the k -means with K_y clusters. Treat each row of \hat{V} as a point in $\mathbb{R}^{n \times K'}$ and run the k -means with K_z clusters.
-

3.2 Consistency

We measure the quality of a clustering algorithm by the misclassification rate. Specifically, for the row clusters, it is defined as

$$\mathcal{L}(Y, \hat{Y}) = \min_{\Psi \in \Psi_{K_y}} \frac{1}{n} \|\hat{Y}\Psi - Y\|_0, \quad (10)$$

where $\hat{Y} \in \{0, 1\}^{n \times K_y}$ and Y correspond to the estimated and true membership matrices with respect to the row clusters, respectively, and Ψ_{K_y} is the set of all $K_y \times K_y$ permutation matrices. Similarly, we can define the misclassification rate with respect to the column clusters by $\mathcal{L}(Z, \hat{Z})$.

To establish theoretical bounds on the misclassification rates, we need to pose assumption on the B_l matrices. We consider the rather general case where the aggregated squared block probability matrices $\sum_{l=1}^L B_l B_l^T$ and $\sum_{l=1}^L B_l^T B_l$ are allowed to be rank-deficient, where only a linear growth of their minimum *non-zero* eigenvalue is required. Specifically, we have the following Assumption 2.

Assumption 2. *The K th ($K \leq K_y$) non-zero eigenvalue of $\sum_{l=1}^L B_l B_l^T$ and the K' th ($K' \leq K_z$) non-zero eigenvalue of $\sum_{l=1}^L B_l^T B_l$ are at least $c_1 L$ for some constant $c_1 > 0$.*

Remark 3. *Compared with literature on multi-layer SBMs, see for example [Arroyo et al. \(2021\)](#); [Lei and Lin \(2023\)](#), Assumption 2 is much weaker. On the one hand, we do not require each B_l being of full rank, which is the benefit of combining layer-wise networks. On the other hand, the combined block probability matrix $\sum_{l=1}^L B_l B_l^T$ is also flexible to be degenerate.*

The following theorem provides an upper bound on the proportion of misclustered nodes in terms of row clusters under the multi-layer ScBM mentioned in Lemma 1.

Theorem 1. *Suppose that Assumptions 1 and 2, and (2) hold. If $L^{1/2} n \rho \geq c_2 \log(L + n)$ and $n \rho \leq c_3$ for positive constants c_2 and c_3 , then the output \hat{Y} of Algorithm 1 satisfies*

$$\mathcal{L}(Y, \hat{Y}) \leq \frac{c_4}{n \zeta_n^2} \left(\frac{1}{n^2} + \frac{\log(L + n)}{L n^2 \rho^2} \right) \quad (11)$$

with probability at least $1 - O((L + n)^{-1})$ for some constant $c_4 > 0$, where recall that ζ_n appears in (2).

The proof of Theorem 1 is given in Appendix B. Theorem 1 shows that in certain sense, the number of layers L can boost the clustering performance. In addition, as expected, large ζ_n would bring benefit to the clustering performance. In particular, if $\sum_{l=1}^L B_l B_l^T$ is of full rank, the RHS of (11) can be simplified to

$$c_5 \left(\frac{1}{n^2} + \frac{\log(L+n)}{Ln^2\rho^2} \right)$$

for some constant $c_5 > 0$.

Remark 4. Define the K th smallest non-zero eigenvalue of $\sum_{l=1}^L B_l B_l^T$ by σ_K . Without specifying the linear growth of σ_K with L as in Assumption 2, the misclassification rate is bounded by

$$\mathcal{L}(Y, \hat{Y}) \leq \frac{c_6}{n\zeta_n^2} \left(\frac{L^2}{n^2\sigma_K^2} + \frac{L\log(L+n)}{\sigma_K^2 n^2\rho^2} \right).$$

It should be noted that when choosing different growth rate of σ_K , the misclassification rate as long as the requirement of ρ to obtain consistency would be modified accordingly.

Remark 5. Note that in (11), we can also replace ζ_n by $\min_{1 \leq k \neq k' \leq K_y} \left\| \frac{Q_{k*}^R}{\sqrt{n_k}} - \frac{Q_{k'*}^R}{\sqrt{n_{k'}}} \right\|_2$, namely, the LHS of (2). We here use ζ_n to emphasize the lower bound of the row distance of eigenvector matrix.

Remark 6. The balances of both the true row and true column clusters (i.e., Assumption 1) are used to simplify the misclassification rate in Theorem 1. Specifically, Assumption 1 is used to provide an explicit lower bound for the minimum non-zero eigenvalues of $\sum_{l=1}^L \mathcal{P}_l \mathcal{P}_l^T$; see details in the proof.

In Theorem 1, we consider a situation where the layer-wise networks are rather sparse, with $n\rho \leq c_3$. This situation is interesting because in the single-layer network clustering problem, a well-known necessary condition for the weak consistency is $n\rho \geq c$ for some constant $c > 0$. In the context of multi-layer networks, the increasing of network layers help to alleviate the requirement for ρ by \sqrt{L} (i.e., $L^{1/2}n\rho \geq c_2 \log(L+n)$). In Proposition 1 of Appendix C, we also establish the misclassification rate under the situation $n\rho \geq c_7 \log(L+n)$. In addition, we show the effect of bias-adjustment in Proposition 2 of Appendix C.

Analogous to the row clusters, we provide the following results on the misclassification rate with respect to the column clusters.

Theorem 2. *Suppose that Assumptions 1 and 2, and (4) hold. If $L^{1/2}n\rho \geq c_8 \log(L+n)$ and $n\rho \leq c_9$ for positive constants c_8 and c_9 , then the output \widehat{Z} of Algorithm 1 satisfies*

$$\mathcal{L}(Z, \widehat{Z}) \leq \frac{c_{10}}{n\xi_n^2} \left(\frac{1}{n^2} + \frac{\log(L+n)}{Ln^2\rho^2} \right)$$

with probability at least $1 - O((L+n)^{-1})$ for some constant $c_{10} > 0$, where we recall that ξ_n appears in (4).

As the proof of Theorem 2 follows a similar approach to that of Theorem 1, it is omitted for brevity. Also, we can similarly discuss the results of Theorem 2.

Remark 7. *In the proofs of Theorems 1 and 2, we assume that the k -means algorithm finds the optimal solution, while we use the heuristic Lloyd’s algorithm to solve k -means in experiments due to its efficiency and satisfactory empirical performance. Alternatively, one can also use a more delicate $(1 + \varepsilon)$ -approximate k -means (Kumar et al., 2004) for a good approximate solution within a constant fraction of the optimal value.*

3.3 Discussion

The theoretical challenges of our method lie in the following aspects. First, our assumptions regarding the rank-deficient connectivity matrices are considerably weaker than Lei and Lin (2023), which further brings two barriers for establishing the Theorems 1 and 2. The first barrier is how the eigenvectors of the population SoG matrix relate to the true clusters. For this purpose, we systematically study the eigen-structure of population SoG matrix in Lemma 1 (resp. Lemma 3) and provide interpretable conditions in Lemma 2 (resp. Lemma 4) under which the eigenvectors of the population SoG matrices would reveal the underlying communities in multi-layer ScBMs. The second barrier lies in how to establish the lower bound of the smallest non-negative eigenvalues of the population SoG matrix. For this purpose, we carefully analyze the lower bound in Lemma 5, which plays a crucial role for establishing the misclassification error bound. Second, the elements of noise term $\sum_{l=1}^L X_l X_l^T - \text{diag}(\sum_{l=1}^L X_l X_l^T)$ exhibit complicated dependence which is caused by

the quadratic form and asymmetry. In order to obtain a sharp bound, we use the decoupling techniques (de la Peña and Montgomery-Smith, 1995; Lei and Lin, 2023) to derive the concentration inequalities of the sum of quadratic asymmetric matrices; see Theorem 3.

4 Simulations

In this section, we evaluate the finite sample performance of the proposed algorithm DSoG. To this end, we perform three experiments. The first one corresponds to the case where $\sum_{l=1}^L B_l B_l^T$ is of full rank, while the second one corresponds to the rank-deficient case. The third one is designed to mimic typical directed network structures.

Methods for comparison. We compare our method DSoG with the following three methods.

- **Sum:** spectral co-clustering based on the *Sum* of adjacency matrices without squaring, that is, taking the left and right singular vectors of $\sum_{l=1}^L A_l$ as input of k -means clustering to obtain row and column clusters, respectively.
- **SoG:** spectral co-clustering based on the *Sum of Gram* matrices, that is, taking the eigenvectors of the non-debiased matrices $\sum_{l=1}^L A_l A_l^T$ and $\sum_{l=1}^L A_l^T A_l$ as the input of k -means clustering to obtain row and column clusters, respectively.
- **MASE:** the method called *Multiple Adjacency Spectral Embedding* (Arroyo et al., 2021), where to obtain row and column clusters, the eigenvectors of $\sum_{l=1}^L U_l U_l^T / L$ and $\sum_{l=1}^L V_l V_l^T / L$ are used as the input of the k -means clustering with U_l and V_l representing the singular vectors of the layer-wise matrices A_l .

Experiment 1. The networks are generated from the multi-layer ScBM via the mechanism given in (1). We consider $n = 500$ nodes per network across $K_y = 3$ row clusters and $K_z = 3$ column clusters, with row cluster sizes $n_1^y = 200$, $n_2^y = 100$, $n_3^y = 200$ and column cluster sizes $n_1^z = 150$, $n_2^z = 200$, $n_3^z = 150$. We fix $L = 50$ and set $B_l = \rho B^{(1)}$ for $l \in \{1, \dots, L/2\}$,

and $B_l = \rho B^{(2)}$ for $l \in \{L/2 + 1, \dots, L\}$, with

$$B^{(1)} = U \begin{bmatrix} 1.5 & 0 & 0 \\ 0 & 0.2 & 0 \\ 0 & 0 & 0.4 \end{bmatrix} V^T \approx \begin{bmatrix} 0.46 & 0.625 & 0.225 \\ 0.46 & 0.225 & 0.625 \\ 0.85 & 0.46 & 0.46 \end{bmatrix}$$

and

$$B^{(2)} = U \begin{bmatrix} 1.5 & 0 & 0 \\ 0 & 0.2 & 0 \\ 0 & 0 & -0.4 \end{bmatrix} V^T \approx \begin{bmatrix} 0.46 & 0.225 & 0.625 \\ 0.46 & 0.625 & 0.225 \\ 0.85 & 0.46 & 0.46 \end{bmatrix},$$

where

$$U = \begin{bmatrix} 1/2 & 1/2 & -\sqrt{2}/2 \\ 1/2 & 1/2 & \sqrt{2}/2 \\ \sqrt{2}/2 & -\sqrt{2}/2 & 0 \end{bmatrix} \quad \text{and} \quad V = \begin{bmatrix} \sqrt{2}/2 & -\sqrt{2}/2 & 0 \\ 1/2 & 1/2 & -\sqrt{2}/2 \\ 1/2 & 1/2 & \sqrt{2}/2 \end{bmatrix}.$$

To measure the effect of network sparsity, we vary the overall edge density parameter ρ in the range of 0.03 to 0.16. It is obvious that direct summation of B_l would lead to the confusion of first and second clusters. Hence, it is expected that **Sum** would not perform well under this case.

Experiment 2. In this experiment, we consider the case where $\sum_{l=1}^L B_l B_l^T$ (or $\sum_{l=1}^L B_l B_l^T$) is rank-deficient. Specifically, we consider the following model. We fix $L = 50$ and set $B_l = \rho B^{(1)}$ for $l \in \{1, \dots, L/2\}$, and $B_l = \rho B^{(2)}$ for $l \in \{L/2 + 1, \dots, L\}$, with

$$B^{(1)} = U \begin{bmatrix} 1.2 & 0 & 0 \\ 0 & 0.4 & 0 \\ 0 & 0 & 0 \end{bmatrix} V^T = \begin{bmatrix} 0.59 & 0.14 & 0.33 \\ 0.14 & 0.39 & 0.47 \\ 0.33 & 0.47 & 0.63 \end{bmatrix}$$

and

$$B^{(2)} = U \begin{bmatrix} 1.2 & 0 & 0 \\ 0 & -0.4 & 0 \\ 0 & 0 & 0 \end{bmatrix} V^T = \begin{bmatrix} 0.01 & 0.46 & 0.52 \\ 0.46 & 0.21 & 0.37 \\ 0.52 & 0.37 & 0.57 \end{bmatrix},$$

where

$$U = V \approx \begin{bmatrix} 0.5 & 0.84 & -0.19 \\ 0.5 & -0.46 & -0.73 \\ 0.71 & -0.27 & 0.65 \end{bmatrix}$$

and ρ is the overall edge density parameter which varies from 0.03 to 0.16. It is easy to see that $\sum_{l=1}^L B_l B_l^T$ is rank-deficient and the rank is 2. As in Experiment 1, we consider $n = 500$ nodes per network across $K_y = 3$ row clusters and $K_z = 3$ column clusters, with row cluster sizes $n_1^y = 100$, $n_2^y = 150$, $n_3^y = 250$ and column cluster sizes $n_1^z = 100$, $n_2^z = 250$, $n_3^z = 150$. With this set-up, we generate the adjacency matrix with respect to each layer via (1).

Experiment 3. In this experiment, we generate directed networks with ‘transmission’ nodes or ‘message passing’ nodes. In networks with ‘transmission’ nodes, there exists a set of nodes that only receive edges from one set of nodes and send edges to another set of nodes, and hence are called ‘transmission nodes’. Hence, the sending clusters and receiving clusters are distinct. See Figure 1 (a) and (b) for illustration. In networks with ‘message passing’ nodes, the edges spanning different communities start in upper communities and extend down to lower communities, just like passing messages. See Figure 1(c) for illustration, where the row clusters and column clusters are identical. In our set-up, we fix $L = 30$ and set $B_l = \rho B^{(1)}$ for $l \in \{1, \dots, L/3\}$, $B_l = \rho B^{(2)}$ for $l \in \{L/3 + 1, \dots, 2L/3\}$, and $B_l = \rho B^{(3)}$ for $l \in \{2L/3 + 1, \dots, L\}$, with

$$B^{(1)} = \begin{bmatrix} 0.3 & 0 & 0 \\ 0 & 0.2 & 0 \\ 0 & 0 & 0.3 \end{bmatrix}, \quad B^{(2)} = \begin{bmatrix} 0 & 0 & 0 \\ 0.3 & 0 & 0 \\ 0.5 & 0.3 & 0 \end{bmatrix}, \quad B^{(3)} = \begin{bmatrix} 0 & 0.2 & 0.2 \\ 0 & 0 & 0.2 \\ 0 & 0 & 0 \end{bmatrix}.$$

Under $B^{(1)}$, we let the row and column clusters to be different with transmission nodes; see Figure 1 (a) and (b) for illustration. Under $B^{(2)}$ and $B^{(3)}$, we incorporate the message passing nodes and the row clusters and column clusters are identical to those corresponds to $B^{(1)}$; see Figure 1 (c) for illustration. Specifically, we consider $n = 300$ nodes per network across $K_y = 3$ row clusters and $K_z = 3$ column clusters, with row cluster sizes $n_1^y = 120$, $n_2^y = 100$, $n_3^y = 80$ and column cluster sizes $n_1^z = 80$, $n_2^z = 100$, $n_3^z = 120$. With this set-up, we generate the adjacency matrix for each layer via (1), with the overall edge density parameter ρ varying from 0.03 to 0.16.

Results. We use the misclassification rate defined in (10) to measure the proportion of misclassified (up to permutations) nodes. The embedding dimensions and the number of

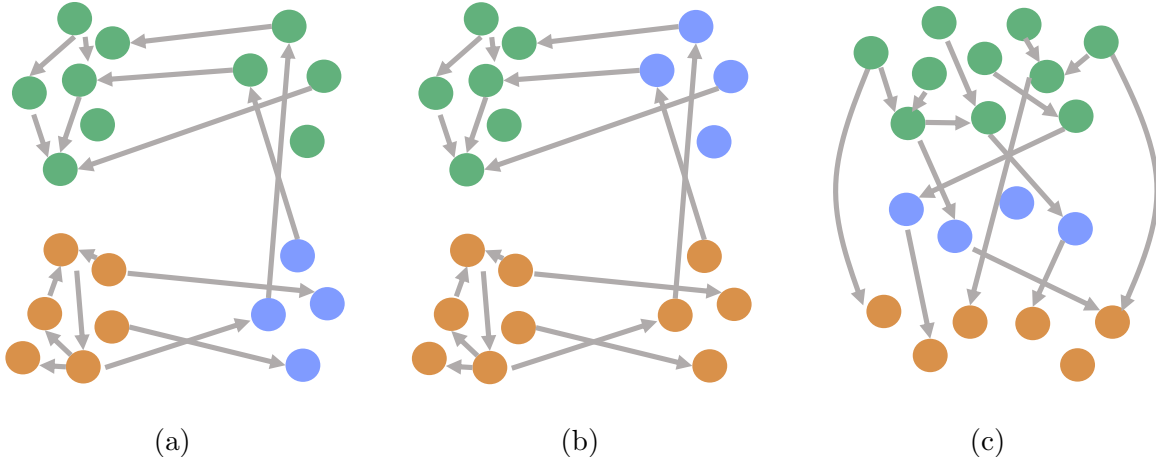


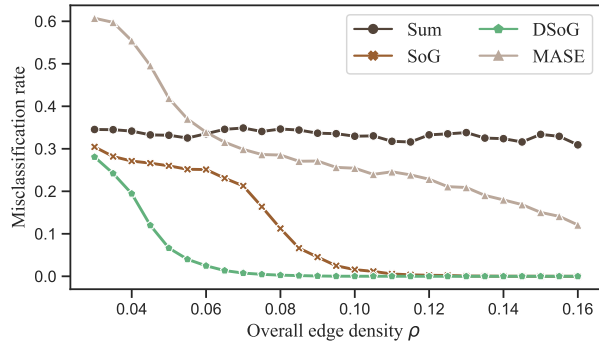
Figure 1: Illustration for networks under different block probability matrices. Colors indicate communities. (a) row clusters under $B^{(1)}$; (b) column clusters under $B^{(1)}$; (c) Row clusters under $B^{(2)}$ ($B^{(3)}$); column clusters are analogous.

clusters are all set to their true values. The averaged results over 50 replications for Experiments 1-3 are displayed in Figure 2, where we vary ρ from 0.03 to 0.16 in 27 equally-spaced values. The results demonstrate that our proposed method DSoG has a noticeable impact on the accuracy of clustering. Specifically, the Sum method performs poorly due to the fact that some eigen-components cancel out in the summation. The DSoG method has a significant advantage over the SoG method, especially when ρ is small, i.e., the very sparse regime, which is consistent with our theoretical results. We can also observe that our method DSoG outperforms the MASE method in all settings.

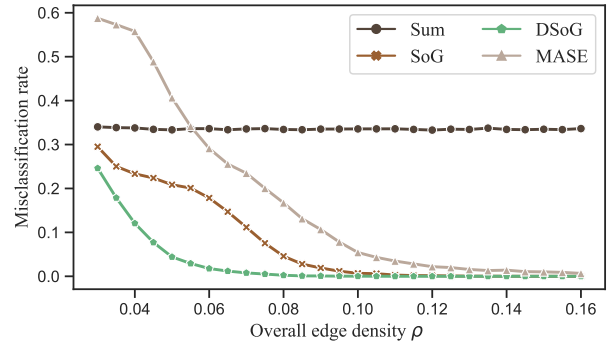
It is important to emphasize that in the above experiments, the community cancellation leads to the inferior performance of Sum, while we note that when the direct summation neither causes community cancellation nor signal reduction, Sum is comparable or slightly better than DSoG. Since we never know the truth in real applications, DSoG provides a safe and satisfactory estimator for co-clustering multi-layer directed networks.

In Appendix E, we also conduct an experiment to study the sensitivity of tuning parameters for each method. It turns out that DSoG continues to outperform other methods, although there exists certain performance degradation for all methods.

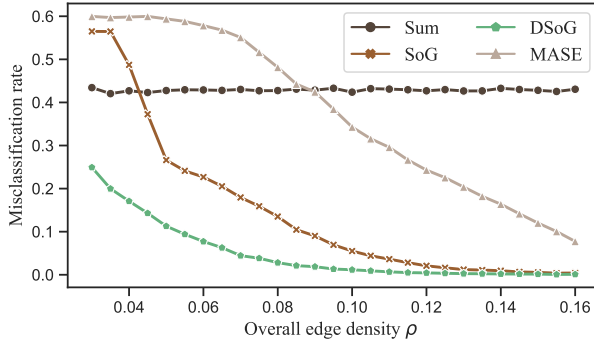
In the above experiments, we focused on the comparison of DSoG with spectral clustering-



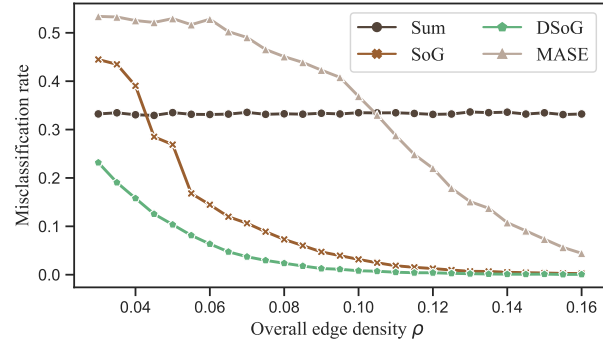
(a) Experiment 1, row clustering



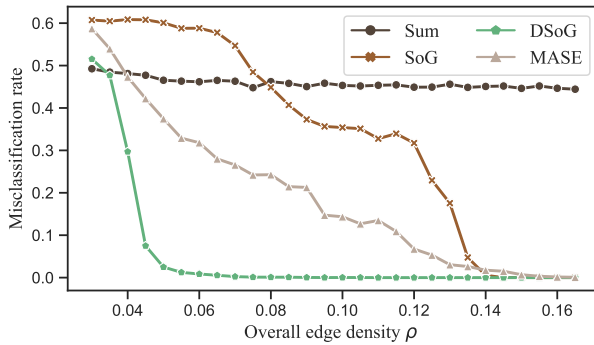
(b) Experiment 1, column clustering



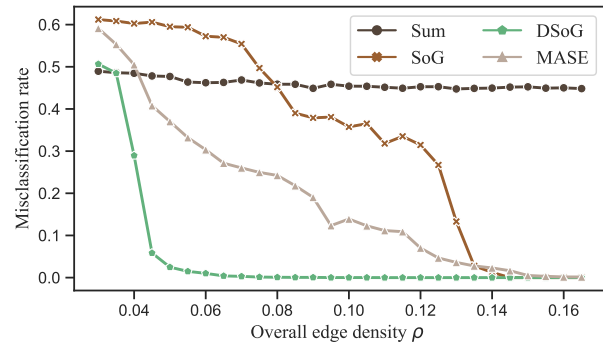
(c) Experiment 2, row clustering



(d) Experiment 2, column clustering



(e) Experiment 3, row clustering



(f) Experiment 3, column clustering

Figure 2: Misclassification rates of four methods with varying ρ in three experimental setups.

based methods. In Appendix E, we also compare DSoG with likelihood-based methods by Wang et al. (2021) and Fu and Hu (2023). It turns out that these likelihood-based methods show unstable and inferior performance under the random initialization or initialized by Sum. While when choosing DSoG as the initial estimator, the likelihood-based method ML-PPL shows better performance than our method DSoG. Hence, the proposed method provides a good initial estimator for these likelihood-based methods when there exists community cancellation via direct summation. In addition, we scale the number of nodes to 1000 and compare the running time of each method. It turns out that DSoG is more computationally efficient than likelihood-based methods. See Appendix E for the detailed experiments and results.

5 Real data analysis

In this section, we analyze the WFAT dataset, which is a public dataset collected by the Food and Agriculture Organization of the United Nations. The original data includes trading records for more than 400 food and agricultural products imported/exported annually by all the countries in the world. The dataset is available at <https://www.fao.org>. As described in other works analyzing these data (De Domenico et al., 2015; Jing et al., 2021; Noroozi and Pensky, 2022), it can be considered as a multi-layer network, where layers represent food and agricultural products, and nodes are countries and edges at each layer represent import/export relationships of a specific food and agricultural product among countries. Specifically, Noroozi and Pensky (2022) treated this dataset as a *mixture* multi-layer SBMs (Pensky and Wang, 2021), that is, the network layers are classified to different groups, the within group layers share common community structures. The method identifies three groups of layers. Therefore, to fit into our assumption that the communities are consensus among layers, we select a group identified by Noroozi and Pensky (2022). This group including 24 products contains mostly cereals, stimulant crops and derived products, see Table 1 for details.

<p> “Pastry”, “Rice, paddy”, “Rice, milled”, “Breakfast cereals”, Mixes and doughs”, “Food preparations of flour, meal or malt extract”, “Sugar and syrups n.e.c.”, “Sugar confectionery”, “Communion wafers and similar products.”, “Prepared nuts”, “Vegetables preserved (frozen)”, “Juice of fruits n.e.c.”, “Fruit prepared n.e.c.”, “Orange juice”, “Other non-alcoholic caloric beverages”, “Food wastes”, “Other spirituous beverages”, “Coffee, decaffeinated or roasted”, “Coffee, green”, “Chocolate products nes”, “Pepper, raw”, “Dog or cat food, put up for retail sale”, “Food preparations n.e.c.”, “Crude organic material n.e.c.” </p>
--

Table 1: List of a group of food and agricultural products we considered, which consists of 24 different products involving cereals, stimulant crops, and derived products.

Data preprocessing. We convert the original trading data into directed networks, which is distinct from all previously described efforts to analyze this data, where the trading data is reduced to an undirected network. We focus on the trading data in the year 2020. To create a directed trading network for each of the 24 products, we draw a directed edge from the exporter to the importer if the export/import value of the product exceeds \$10000. This particular threshold would yield sparse networks that have many disjoint connected components individually but have one connected component after aggregation. It is important to mention that the performance of DSoG is insensitive to the specific product value threshold. We then remove all the countries (nodes) whose total in-degree or out-degree across all 24 layers is less than 14. We choose this value to make sure that each node has links to at least one of the other nodes in at least half of the layers. Indeed, the average total in-degree and out-degree of nodes which do not have any neighbors in 12 or more of the layers (i.e., more than half of the layers have a zero out-degree or in-degree) is 13. As a result, we obtain a multi-layer network with 24 layers and 142 nodes per layer. Subsequently, we reconstruct the row and column clusters using the proposed algorithm.

Tuning parameters selection. There are four tuning parameters K_y, K_z, K and K' in real data analysis. To select the embedding dimensions K and K' , we use the scree plot method, which is widely used in network data analysis. The scree plot of the top eigenvalues

of the debiased SoG matrices over the layer-wise adjacency matrices are shown in Figure 3. For both of the row and column clustering, there is an elbow on the scree plot at the 4th position. Hence, we choose $K = 4$ and $K' = 4$ in the WFAT data analysis.

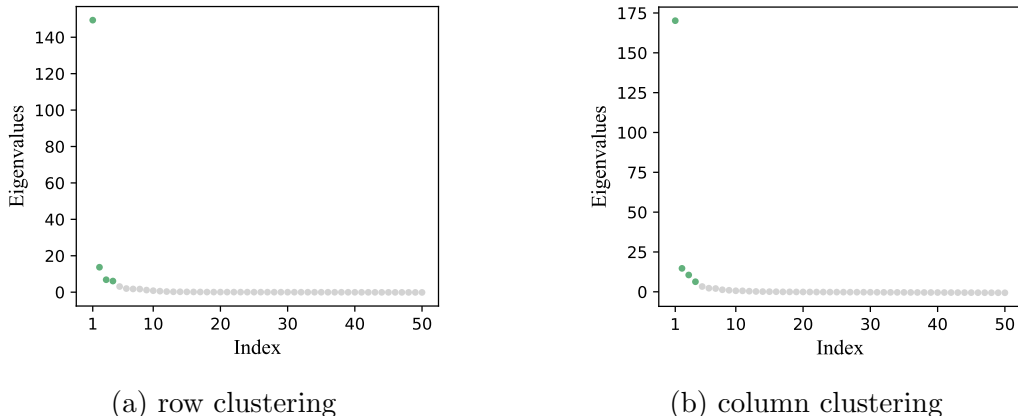


Figure 3: Scree plots of the top eigenvalues of DSoG matrices with respect to row clustering and column clustering for the WFAT data.

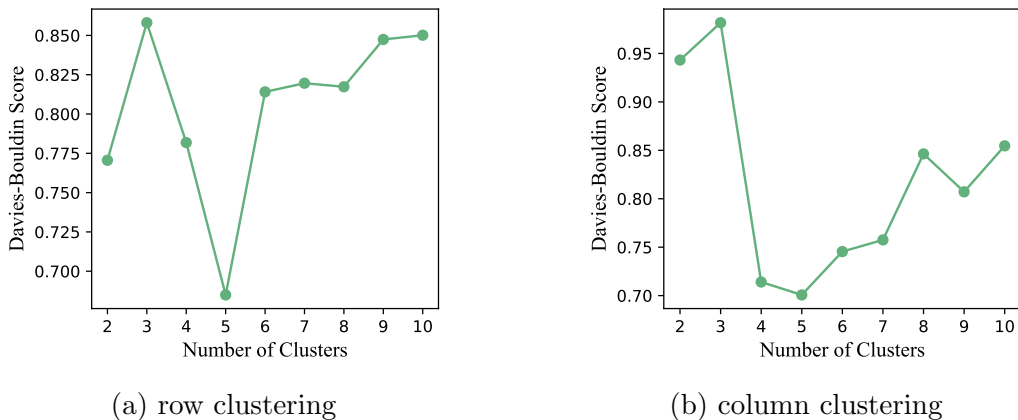


Figure 4: Davies-Bouldin scores under different clustering numbers with respect to row clustering and column clustering for the WFAT data.

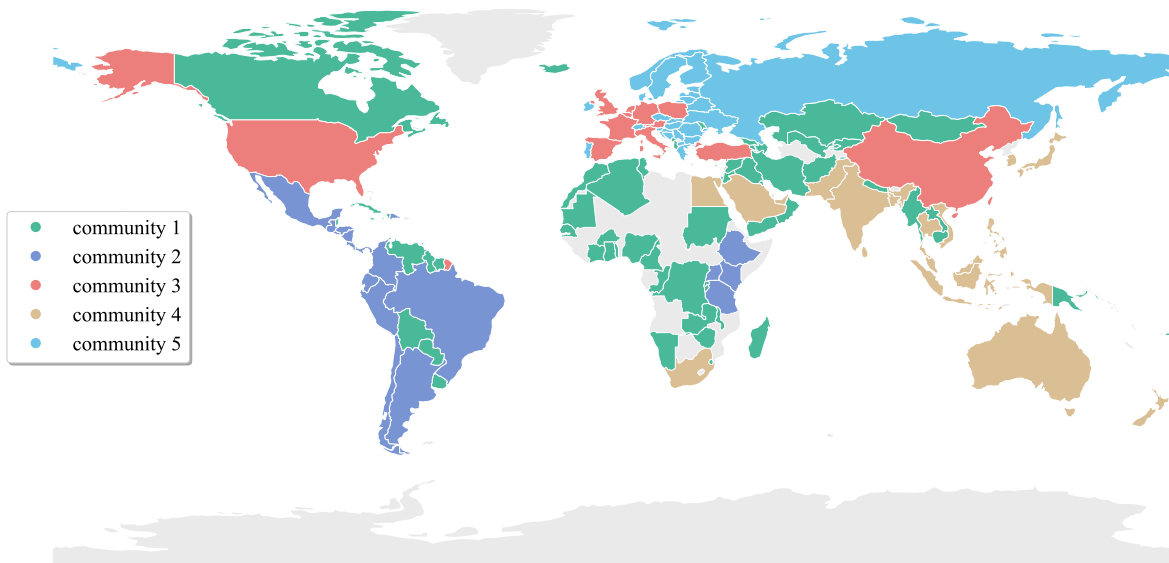
To select the number of clusters K_y and K_z , we use the model-free method Davies-Bouldin score (Davies and Bouldin, 1979), because current literature for selecting the number of clusters violated our rank-deficient assumption (Li et al., 2020; Hu et al., 2020). Figure 4 shows the Davies-Bouldin scores for the row and column clustering, where a smaller value indicates a more compact and well-separated cluster. The Davies-Bouldin scores turn out

to attain their minimum at 5 for both the row and column clustering. Hence, we set $K_y = K_z = 5$ in the WFAT data analysis.

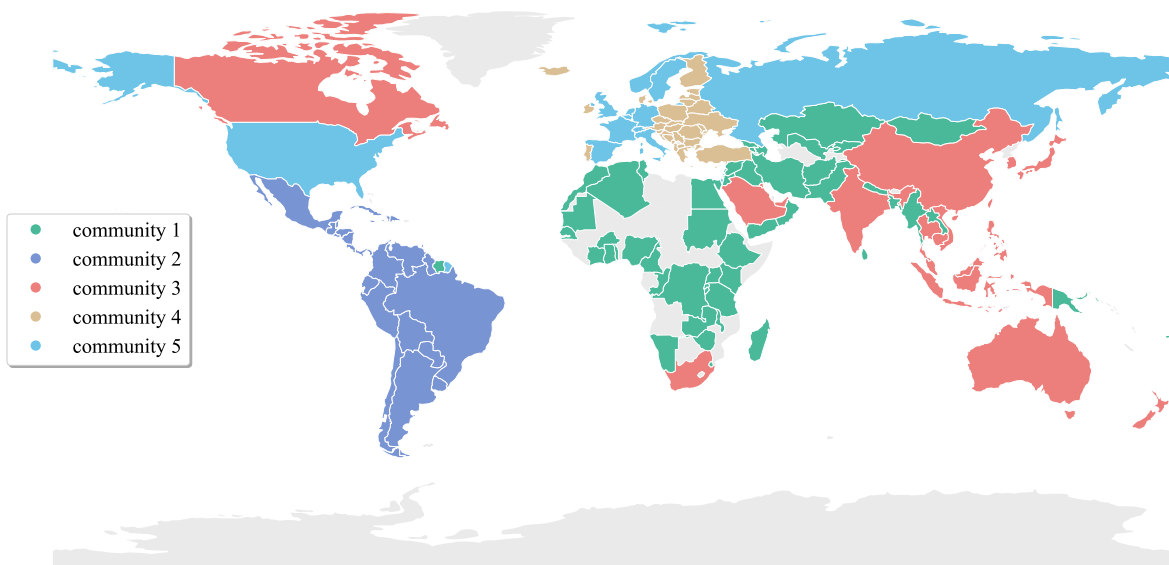
Results. The estimated row and column clusters are displayed in Figure 5. The clusters of countries are approximately related to their geographic locations, which is coherent with the economic laws of world trade. Specifically, for the row clusters (see Figure 5(a)), Community 1 mainly includes countries in Africa, West and Central Asia; Community 2 is composed of countries in Central and South America; Community 3 includes China, the United States, Western and Southern Europe countries; Community 4 involves Southeast Asia and Oceania countries; Community 5 consists of the remaining European countries. For the column clusters (see Figure 5(b)), Community 1 mainly includes Africa and West Asian countries; Community 2 consists of countries in Central and South America; Community 3 includes Oceania, East and South Asian countries; Community 4 involves Eastern European and some West Asian countries; Community 5 mainly includes Western Europe, North America and Russia.

We can see that the structure of the row (export) clusters is not identical to that of the column (import) clusters, which is insightful and more realistic than what would be expected from undirected multi-layer networks. For instance, China is grouped with major European economies and America in the row clusters partition, while it is grouped mainly with East and South Asia countries in the column clusters partition, indicating that for the products in Table 1, China is aligned with major world economies in its export trade, while it is aligned mainly with neighboring countries in its import trade. This observation is entirely plausible. Export patterns primarily reflect a nation’s productive capacity and dominant industries. Major global economies with robust food processing industries and agricultural technology tend to export value-added manufactured goods. Conversely, import patterns primarily mirror a country’s consumer demand. Due to similar geographical conditions, population sizes and food consumption habits, countries in close proximity to each other often exhibit similar import patterns.

By contrast, we compare DSoG with its undirected analog, DSoS. For DSoS, we ignore the direction of edges to obtain symmetrized adjacency matrices A'_i , and then perform eigen-



(a) row (export) clustering



(b) column (import) clustering

Figure 5: Community structure separation of food trade networks (directed) containing 142 major countries. Colors indicate communities, where light gray corresponds to countries that do not participate in clustering.

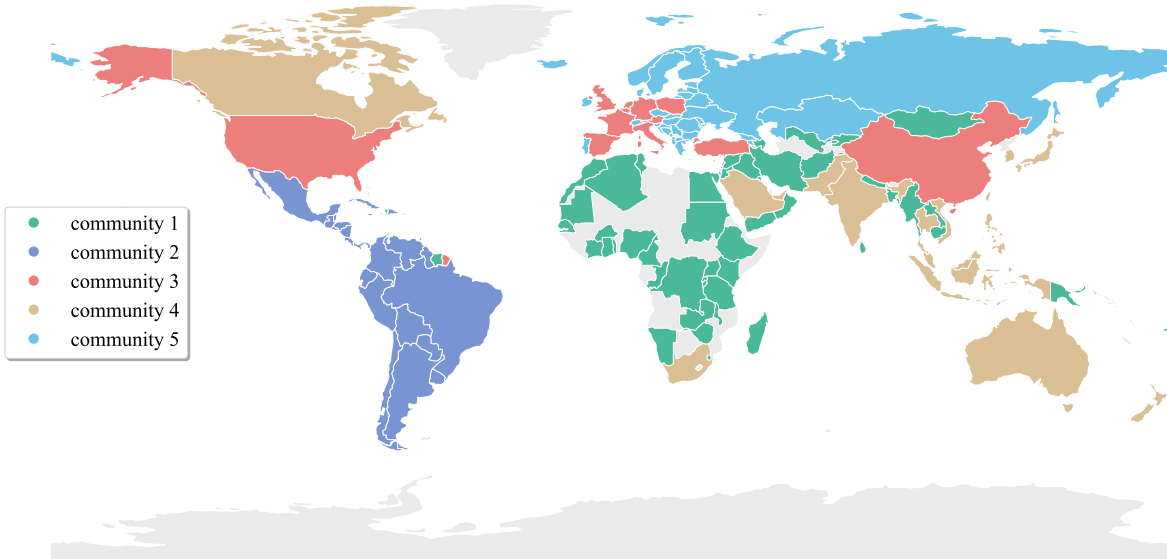


Figure 6: Community structure separation of food trade networks (undirected) containing 142 major countries. Colors indicate communities, where light gray corresponds to countries that do not participate in clustering.

decomposition and k -means on the debiased $\sum_{i=1}^L (A_i')^2$ (Lei and Lin, 2023). The results of DSoS are shown in Figure 6. We use the Adjusted Rand Index (ARI) to measure the similarity between DSoG and DSoS in terms of row clustering and column clustering, where the single set of clusters obtained by DSoS is regarded as both the row and column clusters, and a larger ARI indicates more similarities. It turns out that for the column (import) clusters, the ARI is 0.74, while for the row (export) clusters, the ARI is 0.53. Therefore, the results of DSoS are less aligned with the row clusters of DSoG, which leads to the failure of DSoS in recognizing the export patterns.

Visualizations of the aggregated adjacency matrix and several single-layer adjacency matrices are also presented, which can illustrate the advantages of multi-layer networks and further highlight the difference between sending and receiving patterns. Figure 7 illustrates the network of the products listed in Table 1, aggregated in a summation manner. In Figure 8, the adjacency matrices for the six products featured in Table 1 are displayed. To highlight the clustering outcomes, the order of the nodes (countries) is adjusted accordingly and persists in each plot. Due to space limitations, only a portion of the countries are labeled

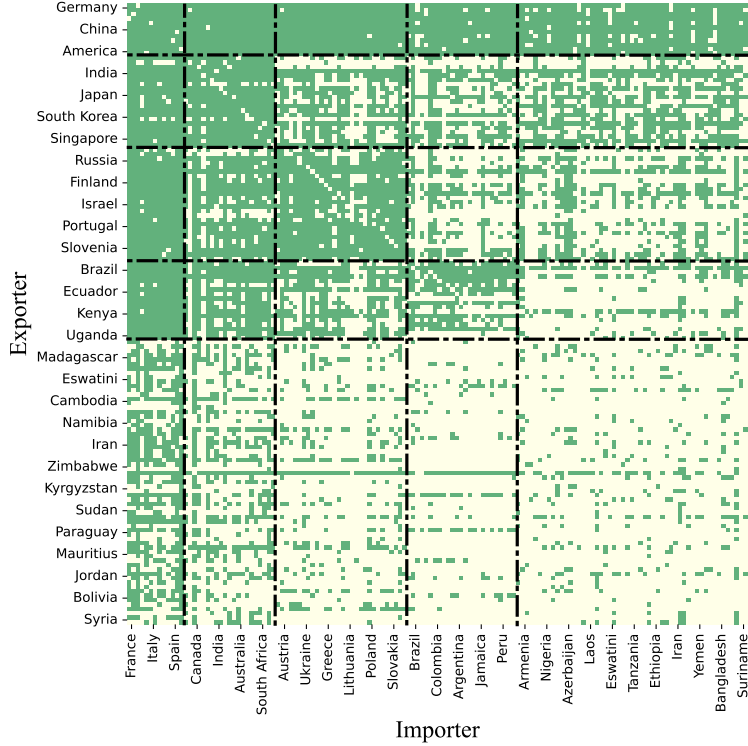
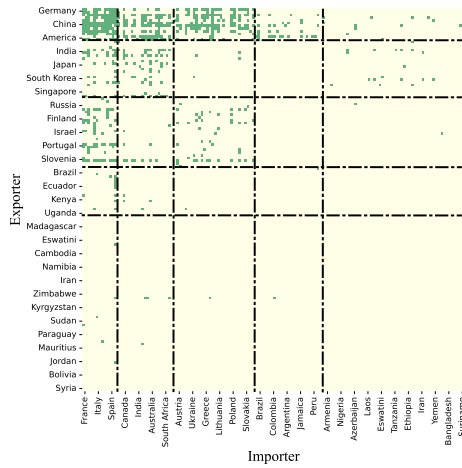


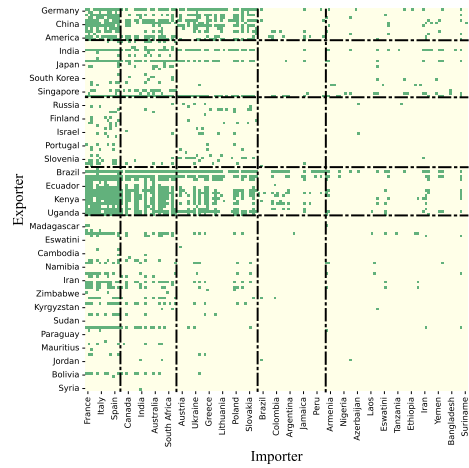
Figure 7: Visualization of the aggregated adjacency matrix. Yellow pixels correspond to the absence of an edge between the corresponding countries while green pixels correspond to an edge. The black dashed lines in the figures signifies the division between clusters.

on the axes. It is clear that our clustering results have a significant community structure, and the row (export) clusters are quite different from the column (import) clusters, as reflected by the fact that the row and column clusters in the same country have distinctly different compositions and different community sizes. Such asymmetric information cannot be captured by undirected networks. More significantly, a comparison between the individual adjacency matrices in Figure 8 and Figure 7 reveals that a single-layer network only encapsulates a fraction of the community structure information, and aggregating the individual trade networks for multiple products provides a more comprehensive picture of trade relations among countries. This aligns with our original intention of dealing with multi-layer directed networks.

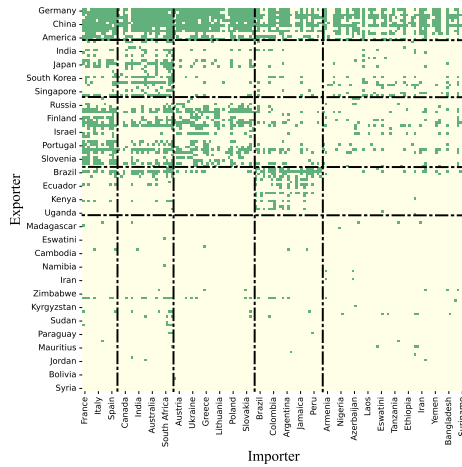
Finally, we highlight the potential loss of cluster divisions through direct aggregation by applying the Sum method to the WFAT data. We also illustrate that a single-layer network is insufficient for comprehensive cluster information by quantifying layer-wise block probability



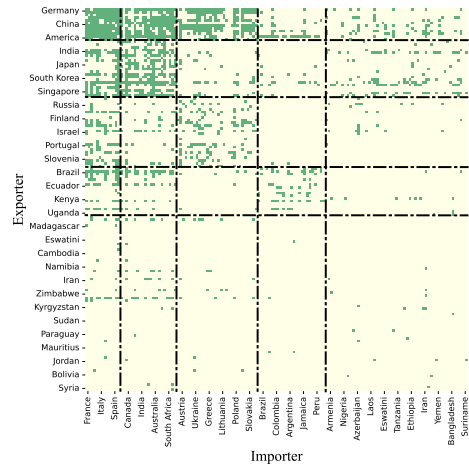
(a) Vegetables preserved (frozen)



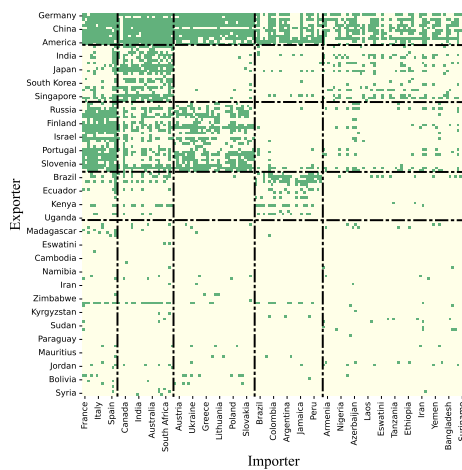
(b) Coffee, green



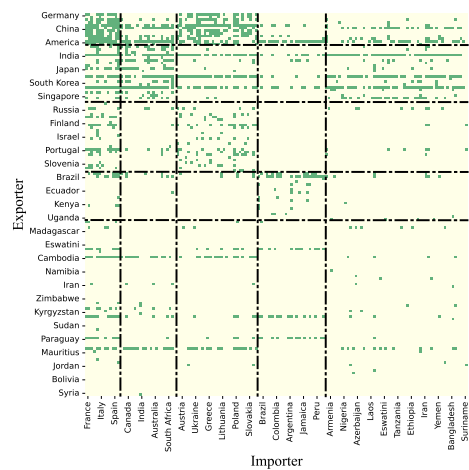
(c) Food wastes



(d) Juice of fruits n.e.c.



(e) Chocolate products nes



(f) Rice, paddy

Figure 8: Visualization of the adjacency matrices for six products. The colors, node order, and community partition are identical to Figure 7.

matrices. See Appendix E for these results. The Python code to run simulations and analysis for this paper is available at <https://github.com/WenqingSu/DSoG>.

6 Conclusion

In this paper, we studied the problem of detecting co-clusters in multi-layer directed networks. We typically assumed that the multi-layer directed network is generated from the multi-layer ScBM, which allows different row and column clusters via different patterns of sending and receiving edges. The proposed method DSoG is formulated as the spectral co-clustering based on the SoG matrices of the row and column spaces, where a bias correction step is implemented. We systematically studied the algebraic properties of the population version of DSoG. In particular, we did not require that the corresponding block probability matrix be of full rank. We also studied the misclassification error rates of DSoG, which show that under certain condition, multiple layers can bring benefit to the clustering performance. We finally conducted numerical experiments on a number of simulated and real examples to support the theoretical results.

There are many ways to extend the content of this paper. First, we focused on the scenario where the layer-wise community structures are homogeneous. It is of great interest to extend the scenario to associated but inhomogeneous community structures, which has been studied recently for multi-layer undirected networks (Han et al., 2015; Pensky and Zhang, 2019; Chen et al., 2022). Second, we analyzed the WFAT dataset with respect to a particular year. However, this dataset contains the annual trading data from 1986 to the present and is continuously updated, which actually constitutes a *higher-order* multi-layer network that contains more adequate information than a single multi-layer network. It is thus of great importance to develop a corresponding toolbox for this higher-order multi-layer network. Third, it is important to theoretically study the estimation of the number of communities (Fishkind et al., 2013; Ma et al., 2021).

Appendix

Appendix A provides the technical theorem and lemma that are needed to prove the misclassification rates. Appendix B includes the proof of main theorem and lemmas in the main text. Appendix C contains additional theoretical results. Appendix D contains auxiliary lemmas. Appendix E provides the additional results for simulation and real data analysis.

A Technical theorem and lemma

Theorem 3. *Let $A_l \in \{0, 1\}^{n \times n}$ be the adjacency matrices generated by a multi-layer ScBM and $X_l = A_l - \bar{P}_l$ be the asymmetric noise matrices for all $1 \leq l \leq L$, where $\bar{P}_l = \mathbb{E}(A_l)$. If $L^{1/2}n\rho \geq c_1 \log(L+n)$ and $n\rho \leq c_2$ for positive constants c_1 and c_2 , then E_1 , the off-diagonal part of $\sum_{l=1}^L X_l X_l^T$, satisfies*

$$\|E_1\|_2 \leq cL^{1/2}n\rho \log^{1/2}(L+n)$$

with probability at least $1 - O((L+n)^{-1})$ for some constant $c > 0$.

To handle the complicated dependence in E_1 caused by the quadratic form, the key idea in the proof is viewing E_1 as a matrix-valued U-statistic with a centered kernel function of order two, indexed by the pairs (i, j) , and using the decoupling technique described in Lemma 8, which reduces problems on dependent variables to problems on related (conditionally) independent variables. This type of proof technique is also used in [Lei and Lin \(2023\)](#), dealing with the symmetric case. Specifically, rearrange E_1 as

$$E_1 = \sum_{l=1}^L \sum_{(i, j) \neq (i', j')} X_{l,ij} X_{l,i'j'} e_i e_{i'}^T I_{\{j=j'\}}, \quad (12)$$

where e_i is the standard basis vector in \mathbb{R}^n and pairs $(i, j), (i', j') \in \{1, 2, \dots, n\}^2$, which can be viewed as a matrix-valued U-statistic defined on the vectors $X_{1,ij}, \dots, X_{L,ij}$ indexed by the pairs (i, j) . The decoupling technique reduces the problem of bounding $\|E_1\|_2$ to that of bounding $\|\sum_{l=1}^L X_l \tilde{X}_l^T\|_2$ and $\|\text{diag}(\sum_{l=1}^L X_l \tilde{X}_l^T)\|_2$, where \tilde{X}_l is an independent copy of X_l for all $1 \leq l \leq L$.

Proof. To use the decoupling argument, define

$$\begin{aligned}\tilde{E}_1 &= \sum_{l=1}^L \sum_{(i,j) \neq (i',j')} X_{l,ij} \tilde{X}_{l,i'j'} e_i e_i^T I_{\{j=j'\}}, \\ \tilde{E}_2 &= \sum_{l=1}^L \sum_{(i,j)} X_{l,ij} \tilde{X}_{l,ij} e_i e_i^T,\end{aligned}$$

and

$$\tilde{E} = \sum_{l=1}^L X_l \tilde{X}_l^T = \tilde{E}_1 + \tilde{E}_2.$$

where \tilde{E}_1 is the zero mean off-diagonal part and \tilde{E}_2 is the diagonal part. Note that $\|\tilde{E}_1\|_2 \leq \|\tilde{E}\|_2 + \|\tilde{E}_2\|_2$, we control the spectral norm of \tilde{E} and \tilde{E}_2 separately.

First step: Controlling \tilde{E} . Recall that $\tilde{X}_l = \tilde{A}_l - \tilde{P}_l$, where \tilde{A}_l is an independent copy of A_l , we reformulate \tilde{E} as

$$\tilde{E} = \sum_{l=1}^L X_l \tilde{X}_l^T = \sum_{l=1}^L X_l \tilde{A}_l^T - \sum_{l=1}^L X_l \tilde{P}_l^T.$$

Applying Lemma 6 with $(v, b) = (2\rho, 1)$, if $L^{1/2}n\rho^{1/2} \geq c_1 \log^{1/2}(L+n)$ for some constant $c_1 > 0$, we have with probability at least $1 - O((L+n)^{-1})$ and universal constant $c > 0$,

$$\left\| \sum_{l=1}^L X_l \tilde{P}_l^T \right\|_2 \leq cL^{1/2}n^{3/2}\rho^{3/2} \log^{1/2}(n+L). \quad (13)$$

Note that the constant c may be different from line to line in this proof.

In order to apply Lemma 6 to control $\sum_{l=1}^L X_l \tilde{A}_l^T$ conditioning on $\tilde{A}_1, \dots, \tilde{A}_L$, we need to upper bound $\max_l \|\tilde{A}_l^T\|_{2,\infty}$, $\sum_{l=1}^L \|\tilde{A}_l^T\|_F^2$ and $\|\sum_{l=1}^L \tilde{A}_l \tilde{A}_l^T\|_2$, respectively. Note that \tilde{A}_l is an independent copy of A_l , now we bound the corresponding version of A_l .

We first consider $\max_l \|A_l^T\|_{2,\infty}$. Note that $\mathbb{E}d_{l,i}^{in} \leq n\rho$. Applying a union bound over $i \in [n]$ and $l \in [L]$, along with the standard Bernstein's inequality

$$\mathbb{P}(d_{l,i}^{in} - \mathbb{E}d_{l,i}^{in} \geq t) \leq \exp\left(-\frac{t^2/2}{n\rho+t}\right)$$

for all $t > 0$, and using the assumption that $n\rho \leq c_2$, then with probability at least $1 - O((L+n)^{-1})$, we have

$$\max_l \|A_l^T\|_{2,\infty} = \max_{l,i} \sqrt{d_{l,i}^{in}} \leq c \log^{1/2}(L+n). \quad (14)$$

For $\sum_{l=1}^L \|A_l^T\|_F^2$, using Bernstein's inequality for $\sum_{l=1}^L d_{l,i}^{in}$ and the assumption that $L^{1/2}n\rho \geq c_1 \log(L+n)$, we have with probability at least $1 - O((L+n)^{-1})$,

$$\sum_{l=1}^L \|A_l^T\|_F^2 \leq n \max_i \sum_{l=1}^L d_{l,i}^{in} \leq cLn^2\rho. \quad (15)$$

Now we turn to $\|\sum_{l=1}^L A_l A_l^T\|_2$. To begin with, decompose $\sum_{l=1}^L A_l A_l^T$ as $F_1 + F_2$, where F_1 is the off-diagonal part, which can be viewed as a matrix-valued U-statistic as in (12), and F_2 is the diagonal part. For the off-diagonal part F_1 , \tilde{F}_1 is defined as the off-diagonal part of $\sum_{l=1}^L A_l \tilde{A}_l^T$ for the purpose of using the decoupling technique. Using symmetrization and Perron-Frobenius theorem, we have

$$\|\tilde{F}_1\|_2 = \left\| \begin{array}{cc} 0 & \tilde{F}_1 \\ \tilde{F}_1^T & 0 \end{array} \right\|_2 \leq \max \left\{ \|\tilde{F}_1\|_{1,\infty}, \|\tilde{F}_1^T\|_{1,\infty} \right\} \leq \max \left\{ \left\| \sum_{l=1}^L A_l \tilde{A}_l^T \right\|_{1,\infty}, \left\| \sum_{l=1}^L \tilde{A}_l A_l^T \right\|_{1,\infty} \right\}.$$

By simple calculations, the l_1 norm of the i th row of $\sum_{l=1}^L A_l \tilde{A}_l^T$ is $\sum_{l=1}^L \sum_{j=1}^n A_{l,ij} \tilde{d}_{l,j}^{in}$. Combining (14) and (15) with Bernstein's inequality, we have

$$\begin{aligned} & \mathbb{P} \left(\sum_{l=1}^L \sum_{j=1}^n A_{l,ij} \tilde{d}_{l,j}^{in} - \sum_{l=1}^L \sum_{j=1}^n \mathbb{E}(A_{l,ij}) \tilde{d}_{l,j}^{in} \geq t \mid \tilde{A}_1, \dots, \tilde{A}_L \right) \\ & \leq \exp \left(- \frac{t^2/2}{cLn^2\rho^2 \log(L+n) + c \log(L+n)t} \right) \end{aligned}$$

for all $t > 0$. By applying the total probability theorem, the union bound, and the assumption that $L^{1/2}n\rho \geq c_1 \log(L+n)$, we have with high probability, $\max_i \sum_{l=1}^L \sum_{j=1}^n A_{l,ij} \tilde{d}_{l,j}^{in} \leq cL^{1/2}n\rho \log(L+n) \leq cLn^2\rho^2$. A similar argument is conducted for $\sum_{l=1}^L \tilde{A}_l A_l^T$. By Lemma 8 we have

$$\|F_1\|_2 \leq cLn^2\rho^2 \quad (16)$$

with high probability. For the diagonal part F_2 , applying (15), we have

$$\|F_2\|_2 = \max_i \sum_{l=1}^L d_{l,i}^{out} \leq cLn\rho \quad (17)$$

with high probability. Combining (16), (17) with the assumption that $n\rho \leq c_2$, we have with probability at least $1 - O((L+n)^{-1})$,

$$\left\| \sum_{l=1}^L A_l A_l^T \right\|_2 \leq cLn\rho.$$

So combining the bounds for $\max_l \|\tilde{A}_l^T\|_{2,\infty}$, $\sum_{l=1}^L \|\tilde{A}_l^T\|_F^2$ and $\|\sum_{l=1}^L \tilde{A}_l \tilde{A}_l^T\|_2$, and applying Lemma 6, we have with probability at least $1 - O((L+n)^{-1})$,

$$\left\| \sum_{l=1}^L X_l \tilde{A}_l^T \right\|_2 \leq cL^{1/2} n \rho \log^{1/2}(L+n).$$

Combining this with (13), we have with probability at least $1 - O((L+n)^{-1})$,

$$\|\tilde{E}\|_2 \leq cL^{1/2} n \rho \log^{1/2}(L+n).$$

Second step: Controlling \tilde{E}_2 . Recall that \tilde{E}_2 is a diagonal matrix whose i th diagonal element is $\sum_{l=1}^L \sum_{j=1}^n X_{l,ij} \tilde{X}_{l,ij}$. Using standard Bernstein's inequality and union bound, we have with probability at least $1 - O((L+n)^{-1})$,

$$\|\tilde{E}_2\|_2 \leq cL^{1/2} n \rho \log^{1/2}(L+n).$$

The claim follows by combining the bounds for $\|\tilde{E}\|_2$ and $\|\tilde{E}_2\|_2$ together with the decoupling inequality in Lemma 8. \square

Lemma 5. *Let H be an $n \times s$ matrix with full column rank and the s th eigenvalue of HH^T is at least h for some constant $h > 0$. Let G be an $s \times s$ symmetric matrix with $\text{rank}(G) = j \leq s$ and the j th eigenvalue of G is at least g for some constant $g > 0$. Then $\lambda_j(HGH^T) \geq hg$.*

Proof. Note that $\text{rank}(H) = s$, we have $\dim\{x \in \mathbb{R}^n \mid x \perp \text{null}(H^T)\} = s$, where $\text{null}(H^T)$ is the nullspace of H^T and is given by $\text{null}(H^T) := \{\theta \in \mathbb{R}^n \mid H^T \theta = 0\}$. Combining this with $\text{rank}(G) = j$, we have $\dim\{x \in \mathbb{R}^n \mid x \perp \text{null}(H^T), H^T x \perp \text{null}(G)\} = s$. Thus

$$\min_{x \in \mathbb{R}^n, x \perp \text{null}(H^T), H^T x \perp \text{null}(G)} \frac{x^T HGH^T x}{x^T x} \geq g \cdot \min_{x \in \mathbb{R}^n, x \perp \text{null}(H^T)} \frac{x^T HH^T x}{x^T x} \geq hg.$$

Applying the Courant-Fischer minimax theorem (Theorem 8.1.2 of Golub and Van Loan (2013)), intersecting on this event, we have

$$\lambda_j(HGH^T) = \max_{\dim(\mathcal{H})=j} \min_{0 \neq x \in \mathcal{H}} \frac{x^T HGH^T x}{x^T x} \geq hg,$$

where \mathcal{H} is the subspace of \mathbb{R}^n . The proof is completed. \square

B Main proofs

Proof of Theorem 1

We decompose the matrix S^R into the sum of a signal term and noise terms.

Recall that $\mathcal{P}_l = \rho Y B_l Z^T$ and $\bar{\mathcal{P}}_l = \mathcal{P}_l - \text{diag}(\mathcal{P}_l)$. Define

$$N_4 = \text{diag}\left(\sum_{l=1}^L X_l X_l^T\right) - \sum_{l=1}^L D_l^{\text{out}}, \quad (18)$$

and recall the definition of S^R in (8) and the decomposition (5), we have

$$S^R = \sum_{l=1}^L \mathcal{P}_l \mathcal{P}_l^T + N_1 + N_2 + N_3 + N_4.$$

We first control the signal term. Recall that $\Delta_z = \text{diag}(\sqrt{n_1^z}, \dots, \sqrt{n_{K_z}^z})$ is a $K_z \times K_z$ diagonal matrix, then $Z = \tilde{Z} \Delta_z$ with \tilde{Z} being a column orthogonal matrix. By the balanced community sizes assumption and the number of column clusters K_z is fixed, the minimum eigenvalue of Δ_z is lower bounded by $c_0 n^{1/2}$ for some constant $c_0 > 1$. Then we have

$$\sum_{l=1}^L \mathcal{P}_l \mathcal{P}_l^T = \rho^2 \sum_{l=1}^L Y B_l \Delta_z \tilde{Z}^T \tilde{Z} \Delta_z B_l^T Y^T \succeq c_0 n \rho^2 Y \left[\sum_{l=1}^L B_l B_l^T \right] Y^T, \quad (19)$$

where \succeq denotes the Loewner partial order, in particular, let A and B be two Hermitian matrices of order p , we say that $A \succeq B$ if $A - B$ is positive semi-definite. Note that Y is of full column rank and the K_y th (and smallest) non-zero eigenvalue of $Y Y^T$ is lower bounded by $c_0 n$ for some constant c_0 , where we used the balanced community sizes assumption and the number of row clusters K_y is fixed. Using Lemma 5 and Assumption 2, we can lower bound the K th eigenvalue of $\sum_{l=1}^L \mathcal{P}_l \mathcal{P}_l^T$ to be

$$\lambda_K\left(\sum_{l=1}^L \mathcal{P}_l \mathcal{P}_l^T\right) \geq c L n^2 \rho^2 \quad (20)$$

for some constant $c > 0$. Note that we use c , c_0 , c_1 and c_2 to represent the generic constants and they may be different from line to line.

Then we bound each noise term respectively. The first noise term N_1 is non-random and satisfies

$$\|N_1\|_2 \leq n \|N_1\|_{\max} \leq L n \rho^2.$$

For N_2 , recalling that $X_l = A_l - \bar{P}_l$, where $X_{l,ij} (1 \leq i, j \leq n)$ is generated independently from centered Bernoulli, and is therefore $(2\rho, 1)$ -Bernstein. Using Lemma 6 and the fact that $\|\bar{P}_l^T \bar{P}_l\|_2 \leq n^2 \rho^2$, $\|\bar{P}_l\|_2 \leq n^2 \rho^2$ and $\|\bar{P}_l\|_{2,\infty} \leq n^{1/2} \rho$, if $L^{1/2} n \rho^{1/2} \geq c_1 \log(L+n)$ for some constant $c_1 > 0$, we have with probability at least $1 - O((L+n)^{-1})$ and universal constant $c > 0$,

$$\|N_2\|_2 \leq c L^{1/2} n^{3/2} \rho^{3/2} \log^{1/2}(n+L).$$

For the noise term N_3 , applying Theorem 3, we have

$$\|N_3\|_2 \leq c L^{1/2} n \rho \log^{1/2}(L+n)$$

with probability at least $1 - O((L+n)^{-1})$.

We next control N_4 . The construction in (7) implies that

$$\|N_4\|_2 \leq L n \rho^2.$$

Let U and \hat{U} be the $n \times K$ matrices consisting of the leading eigenvectors of $\sum_{l=1}^L \mathcal{P}_l \mathcal{P}_l^T$ and S^R , respectively. We are now ready to bound the derivation of \hat{U} from U . Combining the lower bound of signal term and upper bound of all noise terms, we have with high probability,

$$\begin{aligned} \frac{\|N_1 + N_2 + N_3 + N_4\|_2}{\lambda_K(\sum_{l=1}^L \mathcal{P}_l \mathcal{P}_l^T)} &\leq c \frac{L n \rho^2 + L^{1/2} n \rho \log^{1/2}(L+n)}{L n^2 \rho^2} \\ &\leq \frac{c}{n} + \frac{c \log^{1/2}(L+n)}{L^{1/2} n \rho}, \end{aligned}$$

where the first inequality arises from the merging of the N_2 and N_3 terms when $n \rho \leq c_2$ for some constant $c_2 > 0$. By Proposition 2.2 of [Vu and Lei \(2013\)](#) and Davis-Kahan $\sin\Theta$ theorem (Theorem VII.3.1 of [Bhatia \(1997\)](#)), there exists a $K \times K$ orthogonal matrix O such that

$$\begin{aligned} \|\hat{U} - UO\|_F &\leq \sqrt{K} \|\hat{U} - UO\|_2 \\ &\leq \frac{\sqrt{K} \|N_1 + N_2 + N_3 + N_4\|_2}{\lambda_K(\sum_{l=1}^L \mathcal{P}_l \mathcal{P}_l^T) - \|N_1 + N_2 + N_3 + N_4\|_2} \\ &\lesssim \frac{1}{n} + \frac{\log^{1/2}(L+n)}{L^{1/2} n \rho}, \end{aligned}$$

where $a_n \lesssim b_n$ means that there exists some positive constant c such that $a_n \leq c b_n$ for all n . Finally, by using Lemma 7, we are able to obtain the desired bound for the misclassification rate. \square

Proof of Lemma 1

Define $\Delta_y = \text{diag}(\sqrt{n_1^y}, \dots, \sqrt{n_{K_y}^y})$ as a $K_y \times K_y$ diagonal matrix with k th diagonal entry being the l_2 norm of the k th column of Y . Then $Y\Delta_y^{-1}$ is a column orthogonal matrix. Similarly define $\Delta_z = \text{diag}(\sqrt{n_1^z}, \dots, \sqrt{n_{K_z}^z})$. Write \mathcal{P}^R as

$$\begin{aligned} \mathcal{P}^R &= \rho^2 Y \sum_{l=1}^L B_l Z^T Z B_l^T Y^T \\ &= \rho^2 Y \Delta_y^{-1} \Delta_y \sum_{l=1}^L B_l \Delta_z^2 B_l^T \Delta_y \Delta_y^{-1} Y^T = \rho^2 Y \Delta_y^{-1} Q^R D^R Q^{R^T} \Delta_y^{-1} Y^T, \end{aligned}$$

where we used the eigendecomposition of $\Delta_y \sum_{l=1}^L B_l \Delta_z^2 B_l^T \Delta_y$ is $Q^R D^R Q^{R^T}$. Here Q^R is a $K_y \times K$ column orthogonal matrix and D^R is a $K \times K$ diagonal matrix, which is due to the fact that $Z^T Z$ is a positive definite diagonal matrix, and hence the rank of $\sum_{l=1}^L B_l B_l^T$ is equal to the rank of $\Delta_y \sum_{l=1}^L B_l \Delta_z^2 B_l^T \Delta_y$.

It is easy to see that $Y \Delta_y^{-1} Q^R$ has orthogonal columns, so we have

$$U = Y \Delta_y^{-1} Q^R. \quad (21)$$

When $\sum_{l=1}^L B_l B_l^T$ is of full rank, that is, $K = K_y$, $\Delta_y^{-1} Q^R$ is invertible, thus $Y_{i^*} = Y_{j^*}$ if and only if $U_{i^*} = U_{j^*}$. The first claim follows by the fact that the rows of $\Delta_y^{-1} Q^R$ are perpendicular to each other and the k th row has length $\sqrt{n_k^y}$.

When $\sum_{l=1}^L B_l B_l^T$ is rank-deficient, that is, $K < K_y$, $Y_{i^*} = Y_{j^*}$ can also imply $U_{i^*} = U_{j^*}$ by (21). On the other hand, by (21), $\|U_{i^*} - U_{j^*}\|_2 := \left\| \frac{Q_{y_{i^*}}^R}{\sqrt{n_{y_{i^*}}^y}} - \frac{Q_{y_{j^*}}^R}{\sqrt{n_{y_{j^*}}^y}} \right\|_2$. The second claim follows by the rows of $\Delta_y^{-1} Q^R$ are mutually distinct with their minimum Euclidean distance being larger than a deterministic sequence $\{\zeta_n\}_{n \geq 1}$. \square

Proof of Lemma 2

By the balanced community sizes assumption and both K_y and K_z are fixed, we have

$$\Delta_y \sum_{l=1}^L B_l \Delta_z^2 B_l^T \Delta_y \preceq \frac{c_0}{K_z} n \Delta_y \sum_{l=1}^L B_l B_l^T \Delta_y \preceq c_0 K_y L n \Delta_y^2 \preceq c_0^2 L n^2 I_{K_y}, \quad (22)$$

where we used $\Delta_z^2 \preceq \frac{c_0 n}{K_z} I_{K_z}$, $\Delta_y^2 \preceq \frac{c_0 n}{K_y} I_{K_y}$ and $\|\sum_{l=1}^L B_l B_l^T\|_2 \leq L K_y K_z$. Recall that the eigendecomposition of $\Delta_y \sum_{l=1}^L B_l \Delta_z^2 B_l^T \Delta_y$ is $Q^R D^R Q^{R^T}$, (22) implies that D_{kk}^R is upper bounded by $c_0^2 L n^2$ for any $1 \leq k \leq K$.

Define $\mathbb{B}^R := \sum_{l=1}^L B_l \Delta_z^2 B_l^T$, by simple calculations, we have

$$\mathbb{B}_{g_i^y g_j^y}^R = \sum_{k_z=1}^{K_z} \sum_{l=1}^L n_{k_z}^z B_{l, g_i^y k_z} B_{l, g_j^y k_z}$$

for all $1 \leq i, j \leq n$. Under the Assumption 1, it is easy to see that

$$\mathbb{B}_{g_i^y g_j^y}^R \geq \frac{n}{c_0 K_z} \left[\sum_{l=1}^L B_l B_l^T \right]_{g_i^y g_j^y}$$

and

$$\mathbb{B}_{g_i^y g_j^y}^R \leq \frac{c_0 n}{K_z} \left[\sum_{l=1}^L B_l B_l^T \right]_{g_i^y g_j^y}.$$

Let $\mu_n^r := c_0^2 L n^2$, by the decomposition (21), we have

$$\begin{aligned} \mu_n^r \|U_{i^*} - U_{j^*}\|_2^2 &= \sum_{k=1}^K \mu_n^r \left(\frac{Q_{g_i^y k}^R}{\sqrt{n_{g_i^y}}} - \frac{Q_{g_j^y k}^R}{\sqrt{n_{g_j^y}}} \right)^2 \\ &\geq \sum_{k=1}^K D_{kk}^R \left(\frac{Q_{g_i^y k}^R}{\sqrt{n_{g_i^y}}} - \frac{Q_{g_j^y k}^R}{\sqrt{n_{g_j^y}}} \right)^2 \\ &= \sum_{k=1}^K D_{kk}^R \left(\frac{Q_{g_i^y k}^R}{\sqrt{n_{g_i^y}}} \right)^2 + \sum_{k=1}^K D_{kk}^R \left(\frac{Q_{g_j^y k}^R}{\sqrt{n_{g_j^y}}} \right)^2 - 2 \sum_{k=1}^K D_{kk}^R \frac{Q_{g_i^y k}^R Q_{g_j^y k}^R}{\sqrt{n_{g_i^y} n_{g_j^y}}} \\ &= \mathbb{B}_{g_i^y g_i^y}^R + \mathbb{B}_{g_j^y g_j^y}^R - 2 \mathbb{B}_{g_i^y g_j^y}^R \\ &\geq \frac{n}{c_0 K_z} \left[\sum_{l=1}^L B_l B_l^T \right]_{g_i^y g_i^y} + \frac{n}{c_0 K_z} \left[\sum_{l=1}^L B_l B_l^T \right]_{g_j^y g_j^y} - 2 \frac{c_0 n}{K_z} \left[\sum_{l=1}^L B_l B_l^T \right]_{g_i^y g_j^y} \\ &\geq c_0^2 L n^2 \zeta_n^2 \end{aligned}$$

for any $Y_{i^*} \neq Y_{j^*}$. □

Proof of Lemma 3

By the fact that the rank of $\sum_{l=1}^L B_l^T B_l$ is equal to the rank of $\Delta_z \sum_{l=1}^L B_l^T \Delta_z^2 B_l \Delta_z$, we have Q^C is a $K_z \times K$ column orthogonal matrix. It is easy to see that $Z \Delta_z^{-1} Q^C$ has orthogonal columns, so we have

$$V = Z \Delta_z^{-1} Q^C.$$

The rest proof is similar to that of Lemma 1, we omit it here. □

Proof of Lemma 4

The proof of Lemma 4 follows the same strategy as that of Lemma 2. Here we only describe the difference.

Define $\mu_n^c := c_0^2 L n^2$ and $\mathbb{B}^C := \sum_{l=1}^L B_l^T \Delta_y^2 B_l$, by simple calculations, we have

$$\mathbb{B}_{g_i^z g_j^z}^C = \sum_{k_y=1}^{K_y} \sum_{l=1}^L n_{k_y}^z B_{l, k_y g_i^z} B_{l, k_y g_j^z}$$

for all $1 \leq i, j \leq n$. Combining this with Assumption 1 and $V = Z \Delta_z^{-1} Q^C$, we have

$$\begin{aligned} \mu_n^c \|V_{i^*} - V_{j^*}\|_2^2 &\geq \sum_{k=1}^{K'} D_{kk}^C \left(\frac{Q_{g_i^z k}^C}{\sqrt{n_{g_i^z}}} - \frac{Q_{g_j^z k}^C}{\sqrt{n_{g_j^z}}} \right)^2 \\ &= \mathbb{B}_{g_i^z g_i^z}^C + \mathbb{B}_{g_j^z g_j^z}^C - 2\mathbb{B}_{g_i^z g_j^z}^C \\ &\geq \frac{n}{c_0 K_y} \left[\sum_{l=1}^L B_l^T B_l \right]_{g_i^z g_i^z} + \frac{n}{c_0 K_y} \left[\sum_{l=1}^L B_l^T B_l \right]_{g_j^z g_j^z} - 2 \frac{c_0 n}{K_y} \left[\sum_{l=1}^L B_l^T B_l \right]_{g_i^z g_j^z} \\ &\geq c_0^2 L n^2 \xi_n^2 \end{aligned}$$

for any $Z_{i^*} \neq Z_{j^*}$. □

C Additional theoretical results

Proposition 1 provides the misclassification rate of DSoG under a dense regime with $n\rho \geq c_1 \log(L+n)$ for some constant $c_1 > 0$. Proposition 2 provides the misclassification rate of SoG algorithm, namely, the DSoG without the bias-adjustment step.

Proposition 1. *Suppose that Assumptions 1 and 2, and (2) hold. If $n\rho \geq c_1 \log(L+n)$ for some constant $c_1 > 0$, then the output \hat{Y} of Algorithm 1 satisfies*

$$\mathcal{L}(Y, \hat{Y}) \leq \frac{c}{n \zeta_n^2} \left(\frac{1}{n^2} + \frac{\log(L+n)}{Ln\rho} \right)$$

with probability at least $1 - O((L+n)^{-1})$ for some constant $c > 0$.

The proof of this bound is similar to that of Theorem 1, except that Theorem 3 used to control the noise term N_3 is not applicable (alternatively, Theorem 4 of [Lei and Lin \(2023\)](#) can be used), and the upper bound of the noise term N_2 becomes the dominant term.

Proposition 2. *Under the same conditions as in Theorem 1, let \widehat{Y} denote the estimated membership matrices with respect to the row clusters of the SoG method, we have*

$$\mathcal{L}(Y, \widehat{Y}) \leq \frac{c}{n\zeta_n^2} \left(\frac{1}{n^2\rho^2} + \frac{\log(L+n)}{Ln^2\rho^2} \right)$$

with probability at least $1 - O((L+n)^{-1})$ for some constant $c > 0$.

The proof of this bound is similar to that of Theorem 1, except that the upper bound of the noise term N_4 in (18) now satisfies $\|N_4\|_2 \leq c_1 Ln\rho$ with high probability for some positive constant c_1 . The primary improvement of DSoG over SoG is observed in the first term of the upper bound. As a result, when the network is sparse, namely, ρ is small, the bias-adjustment step resulted in a significant reduction in the upper bound of the misclassification rate.

D Auxiliary lemmas

Given a random variable X , we say that Bernstein's condition with parameters v and b holds if $\mathbb{E}[|X|^k] \leq \frac{v}{2} k! b^{k-2}$ for all integers $k \geq 2$. It is also said that X is (v, b) -Bernstein.

Lemma 6 (Theorem 3 in [Lei and Lin \(2023\)](#)). *For $1 \leq l \leq L$, let W_l be a sequence of independent $n \times n$ matrices with zero mean independent entries, and H_l be any sequence of $n \times n$ non-random matrices. If for all $1 \leq l \leq L$ and $1 \leq i, j \leq n$, each entry $W_{l,ij}$ is (v, b) -Bernstein, then for all $t > 0$,*

$$\mathbb{P} \left(\left\| \sum_{l=1}^L W_l H_l \right\|_2 \geq t \right) \leq 4n \exp \left(- \frac{t^2/2}{v \max(n \|\sum_{l=1}^L H_l^T H_l\|_2, \sum_{l=1}^L \|H_l\|_F^2) + b \max_l \|H_l\|_{2,\infty} t} \right).$$

Lemma 7 (Lemma 5.3 in [Lei and Rinaldo \(2015\)](#)). *Let U be an $n \times d$ matrix with K distinct rows with minimum pairwise Euclidean norm separation $\gamma > 0$. Let \widehat{U} be another $n \times d$ matrix and $(\widehat{\Theta}, \widehat{X})$ be an solution to k -means problem with input \widehat{U} , then the number of errors in $\widehat{\Theta}$ as an estimate of the row clusters of U is no larger than $c \|\widehat{U} - U\|_F^2 \gamma^{-2}$ for some constant $c > 0$.*

Lemma 8 (Theorem 1 in [de la Peña and Montgomery-Smith \(1995\)](#)). *Let $\{X_i\}_{i=1}^n$ be a sequence of independent random variables in a measurable space $(\mathcal{S}, \mathcal{S})$, and let $\{X_i^{(j)}\}$, $j = 1, \dots, k$ be k independent copies of $\{X_i\}$. Let $f_{i_1 i_2 \dots i_k}$ be families of functions of k*

variables taking $(\mathcal{S} \times \dots \mathcal{S})$ into a Banach space $(\mathcal{B}, \|\cdot\|)$. Then, for all $n \geq k \geq 2$, $t > 0$, there exist numerical constant $c_k > 0$ depending on k only so that,

$$\begin{aligned} & \mathbb{P}(\| \sum_{1 \leq i_1 \neq i_2 \neq \dots \neq i_k \leq n} f_{i_1 i_2 \dots i_k}(X_{i_1}^{(1)}, X_{i_2}^{(1)}, \dots, X_{i_k}^{(1)}) \| \geq t) \\ & \leq c_k \mathbb{P}(c_k \| \sum_{1 \leq i_1 \neq i_2 \neq \dots \neq i_k \leq n} f_{i_1 i_2 \dots i_k}(X_{i_1}^{(1)}, X_{i_2}^{(2)}, \dots, X_{i_k}^{(k)}) \| \geq t). \end{aligned}$$

E Additional results for simulation and real data analysis

This section presents the additional experimental results that are not shown in the main text.

E.1 Additional results for simulations

Sensitivity of tuning parameters. In Section 4, the tuning parameters for the proposed method DSoG were all set to their true values. Here, we conduct an experiment to show the sensitivity of the selection of tuning parameters. We consider the following rank-deficient multi-layer ScBM. We fix $L = 50$ and set $B_l = \rho B^{(1)}$ for $l \in \{1, \dots, L/2\}$, and $B_l = \rho B^{(2)}$ for $l \in \{L/2 + 1, \dots, L\}$, with

$$B^{(1)} = U \begin{bmatrix} 1.2 & 0 & 0 \\ 0 & 0.4 & 0 \\ 0 & 0 & 0 \end{bmatrix} V^T \approx \begin{bmatrix} 0.287 & 0.293 & 0.326 \\ 0.293 & 0.930 & 0.246 \\ 0.326 & 0.246 & 0.382 \end{bmatrix}$$

and

$$B^{(2)} = U \begin{bmatrix} 1.2 & 0 & 0 \\ 0 & -0.4 & 0 \\ 0 & 0 & 0 \end{bmatrix} V^T \approx \begin{bmatrix} 0.113 & 0.507 & 0.074 \\ 0.507 & 0.670 & 0.554 \\ 0.074 & 0.554 & 0.018 \end{bmatrix},$$

where

$$U = V \approx \begin{bmatrix} 0.408 & 0.467 & -0.784 \\ 0.817 & -0.571 & 0.085 \\ 0.408 & 0.675 & 0.615 \end{bmatrix}.$$

We consider $n = 500$ nodes per network across $K_y = 3$ row clusters and $K_z = 3$ column clusters, with row cluster sizes $n_1^y = 150, n_2^y = 150, n_3^y = 200$ and column cluster sizes

$n_1^z = 150, n_2^z = 200, n_3^z = 150$. In this setup, the true values of the tuning parameters are $K = 2 < K_y = 3$ and $K' = 2 < K_z = 3$. In our experiment, we set $\hat{K} = K_y = 3$ and $\hat{K}' = K_z = 3$, which involves incorrect values of the tuning parameters. The misclassification rates of four methods for different values of ρ are shown in Figure 9. It can be seen that DSoG continues to outperform other methods, although there is certain performance degradation for all methods.

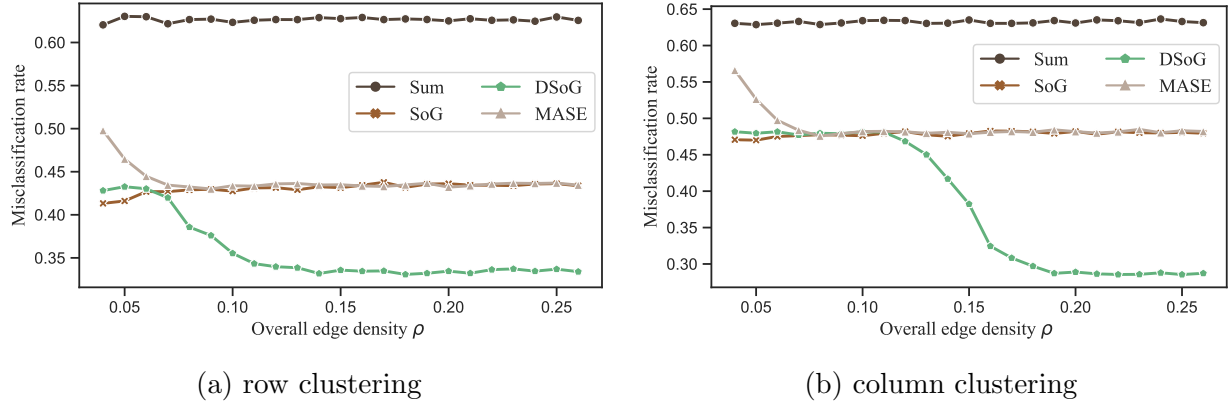
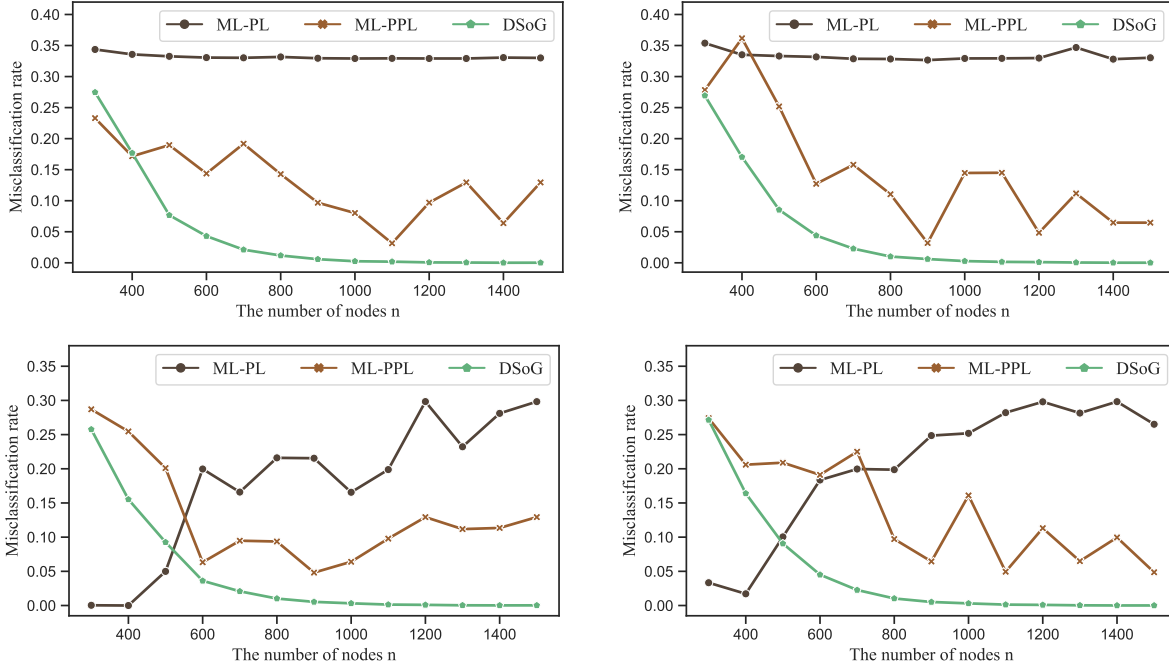
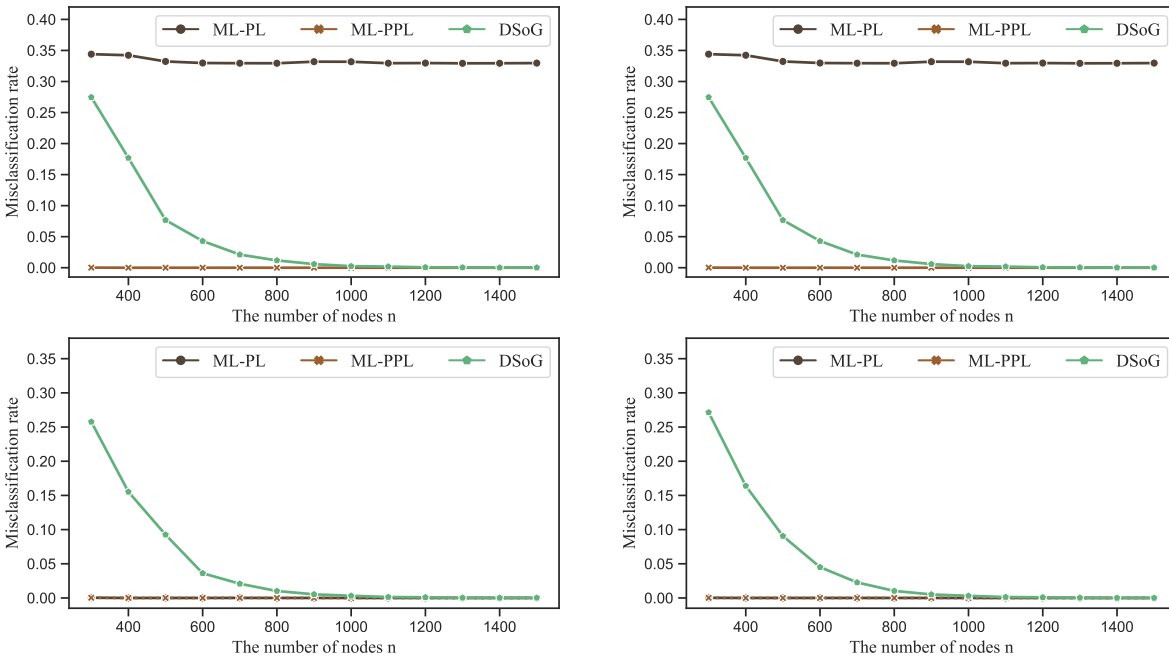


Figure 9: Misclassification rates of four methods in terms of row and column clustering with incorrect selection of tuning parameters.

Comparison with likelihood-based methods. In Section 4, the comparison is limited to spectral clustering-based methods. In addition, likelihood-based methods designed for multi-layer networks, as developed in Wang et al. (2021) and Fu and Hu (2023), are also capable of handling directed networks. Thus, we compare the performance of likelihood-based methods with our proposed approach in the context of multi-layer ScBMs. Specifically, we consider the model from Experiment 1, with the overall edge density $\rho = 0.1$ and the number of network layers $L = 10$. Both the number of row and column communities are set to 3, with balanced community sizes. The number of nodes n varies from 300 to 1500, and the networks are generated from the multi-layer ScBM. Within this setting, we study two different scenarios. In the first scenario, the row and column communities are different, which is the primary interest in co-clustering. In the second scenario, the row and column communities are identical.



(a) ML-PL and ML-PPL with Sum Initialization.



(b) ML-PL and ML-PPL with DSOG Initialization.

Figure 10: Misclassification rates of three methods in terms of row clustering (left panel) and column clustering (right panel) with varying n . The initial values for both ML-PL and ML-PPL are set to the estimates obtained from Sum in (a) and from DSOG in (b), respectively. In both (a) and (b), the row and column membership matrices of the underlying multi-layer ScBM are different (top row) and identical (bottom row).

Since likelihood-based methods are sensitive to initialization, we conduct simulations using two kinds of initial values for these likelihood-based methods. One is the spectral-based method `Sum` which is suggested in Wang et al. (2021) and Fu and Hu (2023), and the other is our method `DSoG`. The averaged misclassification rates over 50 replications are presented in Figure 10, where `ML-PL` denotes the pseudo-likelihood-based algorithm in Wang et al. (2021), and `ML-PPL` denotes the profile-pseudo likelihood-based method in Fu and Hu (2023). It is observed that when initializing with `Sum`, likelihood-based methods are unstable and inferior performance compared to `DSoG`. However, with `DSoG` initialization, the two likelihood-based methods become stable. Particularly in scenarios where row and column communities are identical, the performance of likelihood-based methods is superior. This is not only due to the ability of `ML-PL` and `ML-PPL` to handle directed multi-layer networks, but also due to the proper selection of the initial estimator `DSoG`. In the scenario where row and column communities differ, which is the primary interest in co-clustering, the performance of `ML-PL` is not satisfactory, suggesting that it may not be suitable for handling directed multi-layer networks without specific adjustments.

Efficiency evaluation. In Table 2, we present the average running time of compared algorithms on a directed network with 1000 nodes and 50 layers over 100 replications. These simulations were performed on a PC with an Apple M2 CPU processor. The initial values for `ML-PL` and `ML-PPL` are set as the result of `DSoG`. The results show that the proposed `DSoG` method has the shortest running time, demonstrating its computational efficiency.

Table 2: The running time of four methods on a directed network with 1000 nodes and 50 layers.

Methods	<code>DSoG</code>	<code>MASE</code>	<code>ML-PL</code>	<code>ML-PPL</code>
Running time (s)	6.84	27.18	22.63	34.59

E.2 Additional results for real data analysis

The Sum method for WFAT data. Similar to DSoG, we use the scree plot and the Davies-Bouldin score to select the embedding dimension and the number of clusters. We select the embedding dimension as 2, with $K_y = 4$ and $K_z = 5$ for the respective row and column clusters. Regarding the row clustering, the number of clusters identified by the Sum method is lower compared to the DSoG method, which identified 5 clusters. The row clusters estimated by the Sum method are depicted in Figure 11. Compared to the row clusters estimated by the DSoG method in Figure 5(b), a significant portion of communities 1 and 4 in Figure 5(b) appear to have merged into one single community, indicating a loss of cluster divisions in the summation process.

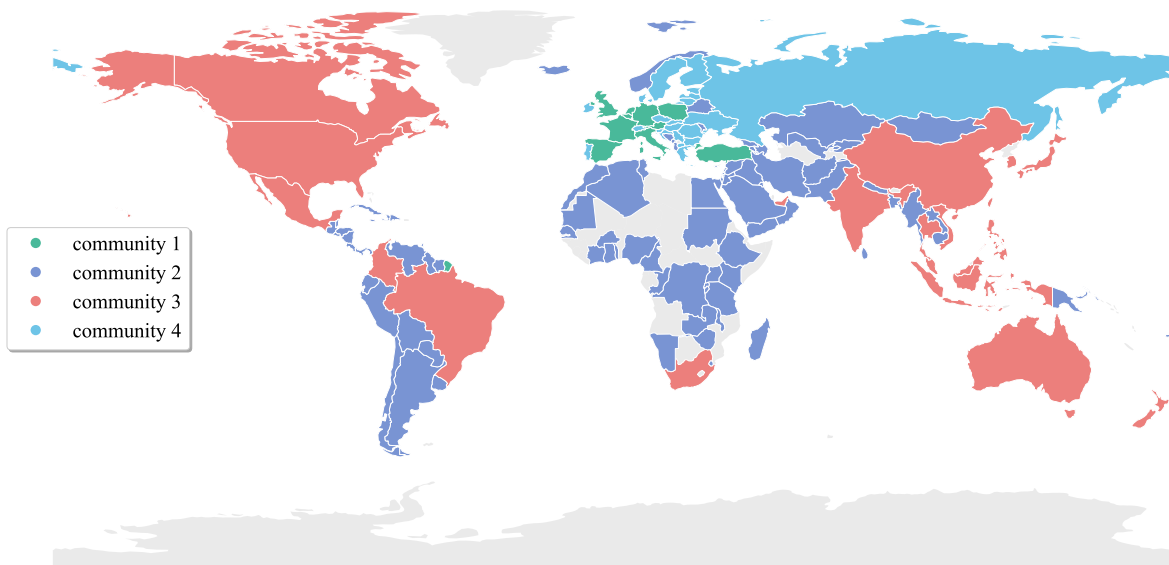


Figure 11: Row community structure separation of food trade networks containing 142 major countries using the Sum method. Colors indicate communities, where light gray corresponds to countries that do not participate in clustering.

Block probability matrices quantification. To complement the analysis provided in Figure 8, we estimate B_l 's in our method to show that the single-layer networks alone are not sufficient to provide complete cluster information. Specifically, we estimate \hat{B}_l by $\hat{B}_l = \hat{Y}^T \hat{\Delta}_y A_l \hat{\Delta}_z \hat{Z}$, where \hat{Y} and \hat{Z} are the estimated row and column membership matrices,

respectively. Both $\hat{\Delta}_y$ and $\hat{\Delta}_z$ are $K \times K$ diagonal matrices with the k th diagonal entry being the l_2 norm of the k th column of \hat{Y} and \hat{Z} , respectively. Figure 12 shows the estimated block probability matrices, which correspond to the products in Figure 8, respectively. It can be seen that for certain layers of networks, the estimated block probability matrices are rank-deficient, indicating that signal for clusters is not strong. For example, for the layer “Vegetables preserved (frozen)” (see Figure 12(a)), the fifth clusters in both the row and column clusters show almost no connections with the other clusters, indicating the vanish of fifth cluster when using this single layer.

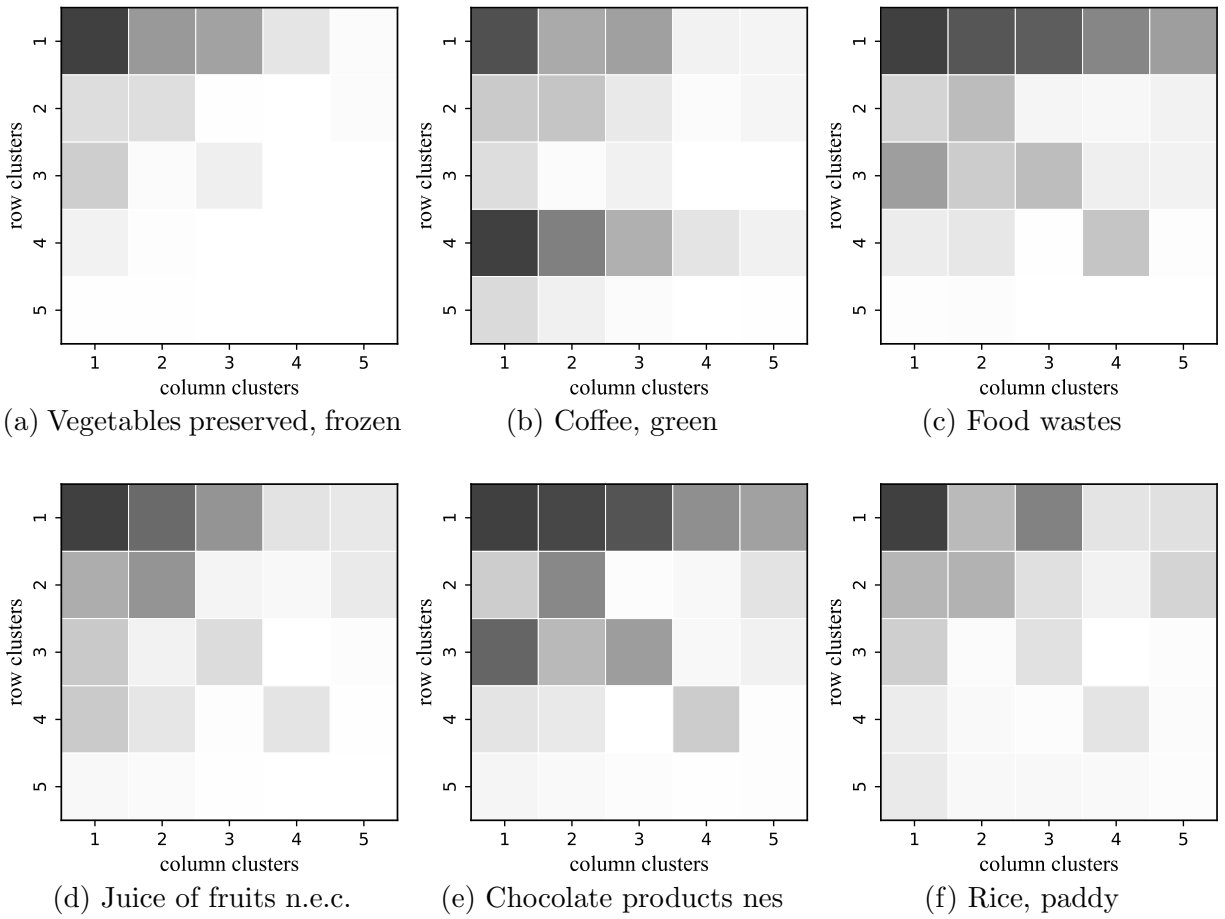


Figure 12: The estimated block probability matrices for six products. Darker colors indicate larger values.

Acknowledgements

The authors are grateful to the editor, associate editor, and two anonymous reviewers for their insightful comments and suggestions.

References

- Arroyo, J., A. Athreya, J. Cape, G. Chen, C. E. Priebe, and J. T. Vogelstein (2021). Inference for multiple heterogeneous networks with a common invariant subspace. *Journal of Machine Learning Research* 22(142), 1–49.
- Bakken, T. E., J. A. Miller, S.-L. Ding, S. M. Sunkin, K. A. Smith, L. Ng, A. Szafer, R. A. Dalley, J. J. Royall, T. Lemon, et al. (2016). A comprehensive transcriptional map of primate brain development. *Nature* 535(7612), 367–375.
- Bhatia, R. (1997). *Matrix analysis*, Volume 169 of *Graduate Texts in Mathematics*. Springer-Verlag, New York.
- Bhattacharyya, S. and S. Chatterjee (2018). Spectral clustering for multiple sparse networks: I. *arXiv preprint arXiv:1805.10594*.
- Boccaletti, S., G. Bianconi, R. Criado, C. I. Del Genio, J. Gómez-Gardenes, M. Romance, I. Sendina-Nadal, Z. Wang, and M. Zanin (2014). The structure and dynamics of multilayer networks. *Physics Reports* 544(1), 1–122.
- Chen, S., S. Liu, and Z. Ma (2022). Global and individualized community detection in inhomogeneous multilayer networks. *The Annals of Statistics* 50(5), 2664–2693.
- Davies, D. L. and D. W. Bouldin (1979). A cluster separation measure. *IEEE transactions on pattern analysis and machine intelligence PAMI-1*(2), 224–227.
- De Domenico, M., V. Nicosia, A. Arenas, and V. Latora (2015). Structural reducibility of multilayer networks. *Nature Communications* 6, 6864.

- de la Peña, V. H. and S. J. Montgomery-Smith (1995). Decoupling inequalities for the tail probabilities of multivariate u-statistics. *The Annals of Probability* 23(2), 806–816.
- Della Rossa, F., L. Pecora, K. Blaha, A. Shirin, I. Klickstein, and F. Sorrentino (2020). Symmetries and cluster synchronization in multilayer networks. *Nature Communications* 11, 3179.
- Fishkind, D. E., D. L. Sussman, M. Tang, J. T. Vogelstein, and C. E. Priebe (2013). Consistent adjacency-spectral partitioning for the stochastic block model when the model parameters are unknown. *SIAM Journal on Matrix Analysis and Applications* 34(1), 23–39.
- Fu, K. and J. Hu (2023). Profile-pseudo likelihood methods for community detection of multilayer stochastic block models. *Stat* 12(1), e594.
- Golub, G. H. and C. F. Van Loan (2013). *Matrix computations*. JHU press, Baltimore.
- Guo, X., Y. Qiu, H. Zhang, and X. Chang (2023). Randomized spectral co-clustering for large-scale directed networks. *Journal of Machine Learning Research* 24(380), 1–68.
- Han, Q., K. Xu, and E. Airoldi (2015). Consistent estimation of dynamic and multi-layer block models. In *International Conference on Machine Learning*, pp. 1511–1520. PMLR.
- Holland, P. W., K. B. Laskey, and S. Leinhardt (1983). Stochastic blockmodels: First steps. *Social Networks* 5(2), 109–137.
- Holme, P. and J. Saramäki (2012). Temporal networks. *Physics Reports* 519(3), 97–125.
- Hu, J., H. Qin, T. Yan, and Y. Zhao (2020). Corrected bayesian information criterion for stochastic block models. *Journal of the American Statistical Association* 115(532), 1771–1783.
- Huang, S., H. Weng, and Y. Feng (2023). Spectral clustering via adaptive layer aggregation for multi-layer networks. *Journal of Computational and Graphical Statistics* 32(3), 1170–1184.

- Jing, B.-Y., T. Li, Z. Lyu, and D. Xia (2021). Community detection on mixture multilayer networks via regularized tensor decomposition. *The Annals of Statistics* 49(6), 3181–3205.
- Kivelä, M., A. Arenas, M. Barthelemy, J. P. Gleeson, Y. Moreno, and M. A. Porter (2014). Multilayer networks. *Journal of Complex Networks* 2(3), 203–271.
- Kumar, A., Y. Sabharwal, and S. Sen (2004). A simple linear time $(1 + \varepsilon)$ -approximation algorithm for k -means clustering in any dimensions. In *45th Annual IEEE Symposium on Foundations of Computer Science*, pp. 454–462. IEEE.
- Lei, J., K. Chen, and B. Lynch (2020). Consistent community detection in multi-layer network data. *Biometrika* 107(1), 61–73.
- Lei, J. and K. Z. Lin (2023). Bias-adjusted spectral clustering in multi-layer stochastic block models. *Journal of the American Statistical Association* 118(544), 2433–2445.
- Lei, J. and A. Rinaldo (2015). Consistency of spectral clustering in stochastic block models. *The Annals of Statistics* 43(1), 215–237.
- Li, T., E. Levina, and J. Zhu (2020). Network cross-validation by edge sampling. *Biometrika* 107(2), 257–276.
- Ma, S., L. Su, and Y. Zhang (2021). Determining the number of communities in degree-corrected stochastic block models. *Journal of Machine Learning Research* 22(310), 1–61.
- MacDonald, P. W., E. Levina, and J. Zhu (2022). Latent space models for multiplex networks with shared structure. *Biometrika* 109(3), 683–706.
- Malliaros, F. D. and M. Vazirgiannis (2013). Clustering and community detection in directed networks: A survey. *Physics Reports* 533(4), 95–142.
- Mucha, P. J., T. Richardson, K. Macon, M. A. Porter, and J.-P. Onnela (2010). Community structure in time-dependent, multiscale, and multiplex networks. *Science* 328(5980), 876–878.
- Noroozi, M. and M. Pensky (2022). Sparse subspace clustering in diverse multiplex network model. *arXiv preprint arXiv:2206.07602*.

- Paul, S. and Y. Chen (2016). Consistent community detection in multi-relational data through restricted multi-layer stochastic blockmodel. *Electronic Journal of Statistics* 10(2), 3807–3870.
- Paul, S. and Y. Chen (2020). Spectral and matrix factorization methods for consistent community detection in multi-layer networks. *The Annals of Statistics* 48(1), 230—250.
- Pensky, M. and Y. Wang (2021). Clustering of diverse multiplex networks. *arXiv preprint arXiv:2110.05308*.
- Pensky, M. and T. Zhang (2019). Spectral clustering in the dynamic stochastic block model. *Electronic Journal of Statistics* 13(1), 678–709.
- Rohe, K., T. Qin, and B. Yu (2016). Co-clustering directed graphs to discover asymmetries and directional communities. *Proceedings of the National Academy of Sciences* 113(45), 12679–12684.
- Tang, M., J. Cape, and C. E. Priebe (2022). Asymptotically efficient estimators for stochastic blockmodels: The naive mle, the rank-constrained mle, and the spectral estimator. *Bernoulli* 28(2), 1049–1073.
- Valles-Catala, T., F. A. Massucci, R. Guimera, and M. Sales-Pardo (2016). Multilayer stochastic block models reveal the multilayer structure of complex networks. *Physical Review X* 6(1), 011036.
- Vu, V. Q. and J. Lei (2013). Minimax sparse principal subspace estimation in high dimensions. *The Annals of Statistics* 41(6), 2905–2947.
- Wang, J., J. Guo, and B. Liu (2021). A fast algorithm for integrative community detection of multi-layer networks. *Stat* 10(1), e348.
- Zhang, J. and J. Cao (2017). Finding common modules in a time-varying network with application to the drosophila melanogaster gene regulation network. *Journal of the American Statistical Association* 112(519), 994–1008.

Zhang, J., X. He, and J. Wang (2022). Directed community detection with network embedding. *Journal of the American Statistical Association* 117(540), 1809–1819.